San Jose State University
SJSU ScholarWorks

Faculty Research, Scholarly, and Creative Activity

1-1-2022

Spatiotemporally heterogeneous deformation, indirect tectonomagmatic links, and lithospheric evolution during orogenic activity coeval with an arc flare-up

Snir Attia
New Mexico Bureau of Geology and Mineral Resources

Scott R. Paterson
University of Southern California

Dazhi Jiang
Western University

Robert B. Miller
San Jose State University, robert.b.miller@sjsu.edu

Follow this and additional works at: https://scholarworks.sjsu.edu/faculty_rsca

Recommended Citation

Snir Attia, Scott R. Paterson, Dazhi Jiang, and Robert B. Miller. "Spatiotemporally heterogeneous deformation, indirect tectonomagmatic links, and lithospheric evolution during orogenic activity coeval with an arc flare-up" *Geosphere* (2022): 1752-1782. https://doi.org/10.1130/GES02478.1

This Article is brought to you for free and open access by SJSU ScholarWorks. It has been accepted for inclusion in Faculty Research, Scholarly, and Creative Activity by an authorized administrator of SJSU ScholarWorks. For more information, please contact scholarworks@sjsu.edu.

Research Paper

GEOSPHERE

GEOSPHERE, v. 18, no. 6

https://doi.org/10.1130/GES02478.1

12 figures; 3 tables; 1 set of supplemental files

CORRESPONDENCE: snir.attia@nmt.edu

CITATION: Attia, S., Paterson, S.R., Jiang, D., and Miller, R.B., 2022, Spatiotemporally heterogeneous deformation, indirect tectonomagmatic links, and lithospheric evolution during orogenic activity coeval with an arc flare-up: Geosphere, v. 18, no. 6, p. 1752–1782, https://doi.org/10.1130/GES02478.1.

Science Editor: Andrea Hampel
Associate Editor: Valerio Acocella

Received 11 August 2021
Revision received 1 June 2022
Accepted 11 July 2022

Published online 23 September 2022

GOLD OPEN ACCESS

THE GEOLOGICAL SOCIETY OF AMERICA®

This paper is published under the terms of the CC-BY-NC license.

© 2022 The Authors

Spatiotemporally heterogeneous deformation, indirect tectonomagmatic links, and lithospheric evolution during orogenic activity coeval with an arc flare-up

Snir Attia[1], Scott R. Paterson[2], Dazhi Jiang[3], and Robert B. Miller[4]

[1]New Mexico Bureau of Geology and Mineral Resources, New Mexico Institute of Mining and Technology, Socorro, New Mexico 87801, USA
[2]Department of Earth Sciences, University of Southern California, Los Angeles, California 90089, USA
[3]Department of Earth Sciences, Western University, London, Ontario N6A 5B7, Canada
[4]Geology Department, San Jose State University, San Jose, California 95192, USA

ABSTRACT

Broad overlap between deformation and magmatism in active margins has spurred the development of a conceptual framework of direct tectonomagmatic links in both active and ancient arcs. Although widespread and highly influential, such models have only rarely been critically evaluated. Rigorously linking tectonism, geodynamics, lithospheric evolution, and arc activity requires detailed reconstructions of the spatiotemporal patterns of magmatism and deformation across both a sufficiently wide area and a range of observational scales. Herein, new constraints on the timing, extent, and characteristics of deformation during mid-Cretaceous tectonism in the central Sierra Nevada (eastern California, USA) are synthesized with published geologic mapping, structural studies, and geochronology to create an updated reconstruction of one of the type examples of a hot, magma-rich orogen. Tilted strata, tectonic fabrics, and shear zones with variable geometries, kinematics, intensity, and timing reveal a significantly revised record of ~25 m.y. of heterogeneous deformation ca. 105–80 Ma. Deformation and magmatism show distinct and unrelated spatiotemporal patterns throughout this orogenic episode. Contrary to previous models of direct tectonomagmatic links, many of which were developed in the central Sierra Nevada, arc activity did not control the location, intensity, or kinematics of intra-arc deformation, nor did shear zones control the location of magmatism. Furthermore, arc lithosphere appears to have strengthened, rather than weakened, as the arc-orogenic flare-up proceeded. In addition to changing plate-scale boundary conditions, lithospheric-scale rheological evolution likely played a key role in the patterns of Late Cretaceous deformation observed across strike of the entire Cordilleran margin.

INTRODUCTION

Heterogeneous, non-steady-state deformation at multiple scales is ubiquitous in both active and ancient convergent margin systems (e.g., DeCelles, 2004; Miller et al., 2006; Kokkalas and Aydin, 2013; Schmidt and Platt, 2018). Broad overlap between intra-arc deformation and magmatism (Hamilton, 1969; Burchfiel and Davis, 1972; Tobisch et al., 1995; Paterson and Miller, 1998; Tibaldi et al., 2010; Acocella, 2014) has led to the development of a conceptual framework of direct tectonomagmatic links in arcs wherein these processes control and facilitate one another. Although highly influential in subsequent work on magmatic systems, these models have not been rigorously tested at appropriate scales of observation against detailed reconstructions of tectonic and magmatic activity in exhumed arcs. Such reconstructions require multidisciplinary syntheses spanning a data-rich and well-studied region because arc lithospheric processes are exceptionally dynamic, displaying complex spatiotemporal patterns and continuously modifying the bounding conditions that shape their expression.

Arcs are the site of voluminous continental crust formation and extensive reworking of the lithosphere from the surface to the mantle wedge, with deformation playing a key role in this physical-chemical evolution (Taylor and McLennan, 1995; Hildreth and Moorbath, 1988; Asmerom et al., 1991; Paterson and Miller, 1998; Ducea and Barton, 2007; DeCelles et al., 2009; Paterson and Ducea, 2015; Cao and Paterson, 2016; Sauer et al., 2017; Attia et al., 2020; Ma et al., 2022). Crustal thickening, arc root growth and loss, exhumation, and surface uplift as well as orogen-normal migration of the arc thermal and magmatic axes operate at rates of as much as kilometers per million years (Chen and Moore, 1982; Paterson and Tobisch, 1992; Kay et al., 2005; Cecil et al., 2012, 2018; Rusmore et al., 2013; Cao and Paterson, 2016; Ardill et al., 2018). Magma addition is episodic on time scales of tens of millions of years in these "hot" arc orogens, reaching peak rates of hundreds of cubic kilometers per million years and displaying no apparent relationship between subduction dynamics and arc activity (Ducea, 2001; Acocella and Funiciello, 2010; Paterson et al., 2011; Ward et al., 2014; Kirsch et al., 2016; Cecil et al., 2018; Yang et al., 2020; Chapman et al., 2021).

A variety of processes in arc orogens may substantially modify the strength of the lithosphere. Structures and anisotropy formed in older arcs and orogens can represent inherited tectonic and petrological imprints that persist for hundreds of millions of years (Kistler and Peterman, 1978; Tobisch and Fiske, 1982; Tobisch and Paterson, 1988; Lackey et al., 2008, 2012; Chapman and Ducea, 2019). Magmatic additions and root loss or formation can dramatically change the bulk

Snir Attia https://orcid.org/0000-0001-8582-8197

Downloaded from http://pubs.geoscienceworld.org/gsa/geosphere/article-pdf/18/6/1752/5737985/ges02478.1.pdf
by San Jose State Univ King Library Periodicals user

composition of the lithosphere. Additions of heat and volatiles from magma and tectonic burial and/or exhumation drive metamorphism and alteration. Multiple overlapping magma pulses, which are individually transient local phenomena, can continuously maintain hot melt-rich domains in some small, shifting fraction of the middle to upper crust (Paterson et al., 2011; Gelman et al., 2013; Karakas et al., 2017). Upon freezing, however, magmas become competent, plagioclase-dominated, essentially isotropic additions to the crust (Paterson and Tobisch, 1988). Effective viscosities within arcs span more than 20 orders of magnitude and vary significantly through time across the three-dimensional lithospheric column (Cruden, 1990; Paterson and Fowler, 1993; Tomek et al., 2017). Such rheological variation over the vast range of scales separating microstructures from tectonic plates (~10^{-6} to ~10^{6} m) leads to multiscale deformation partitioning (Lister and Williams, 1983; Jiang and Williams, 1999; Jones et al., 2005; Yonkee and Weil, 2015). These spatiotemporally heterogeneous impacts of lithospheric processes, both dynamic and rheological effects that are herein collectively referred to as the structural impacts of arc activity, are expected to cause extensively partitioned and non-steady-state deformation across all scales of structural development (e.g., Jiang, 2014).

Within the broader Sierra Nevada arc (eastern California, USA), the central Sierra Nevada (CSN) preserves an exceptional record of a ca. 105–80 Ma orogenic episode broadly coeval with a ca. 120–85 Ma arc flare-up (Fig. 1; Bateman, 1992; Tobisch et al., 1995; Cao et al., 2015; Attia et al., 2020). These Cretaceous tectonic and magmatic events represent the culmination of multiple Permian–Cretaceous phases of Cordilleran arc and orogenic activity (Fig. 2; Armstrong and Ward, 1993; Cao et al., 2015; Saleeby and Dunne, 2015; Kirsch et al., 2016; Cecil et al., 2019). The mid-Cretaceous orogenic episode that we focus on herein was characterized by multiscale deformation partitioning, resulting in fabrics and structures with varying geometries, intensity, timing of development, and interpreted kinematics (Tobisch et al., 1977; Jiang and Bentley, 2012; Nadin et al., 2016). The broad spatiotemporal coincidence of this deformation with high-volume magmatism led previous workers to propose direct links between the distribution of deformation and magmatism in time and space as well as direct links between the tectonomagmatic evolution of the CSN and paleotectonic boundary conditions. Many of these hypotheses have been incorporated as fundamental assumptions underpinning subsequent studies of magmatic systems across the world (e.g., Kokkalas and Aydin, 2013; Acocella, 2014; Sheldrake et al., 2020).

For example, Tobisch et al. (1995) proposed an eastward migration of deformation across the CSN throughout the mid-Cretaceous, with the locus of shear-zone activity tracking the migrating magmatic and thermal axes of arc activity. This speculative deformation migration was also thought to have been accompanied by a transition in kinematics from intra-arc contraction to dextral transpression directly due to increasingly oblique subduction occurring either ca. 100–90 Ma or ca. 110–100 Ma (Engebretson et al., 1985; Greene and Schweickert, 1995; Cao et al., 2015; Nadin et al., 2016). These hypotheses have been further extended in subsequent work, which proposed that both the partitioning of transcurrent motion into arcs and intra-arc deformation migration are generally driven by thermomechanical weakening accompanying magmatic activity and may in turn accommodate further magma ascent (e.g., Tikoff and de Saint Blanquat, 1997; de Saint Blanquat et al., 1998; Cooke et al., 2020). Older models invoking arc-normal extension to make space for voluminous pluton emplacement (Tobisch et al., 1986, 1995; Bateman, 1992) were largely abandoned (Tobisch et al., 2000). Instead, mid-Cretaceous pluton emplacement coeval with contraction and/or transpression has been proposed to have occurred along dilational jogs or pull-apart voids within dextral strike-slip or transpressional shear zones related to oblique convergence (Glazner, 1991; Tikoff and Teyssier, 1992; Titus et al., 2005; Bartley et al., 2018). Alternatively, a variety of material-transfer processes, such as stoping and return flow, may accommodate downward transfer of host rocks at a wide range of scales in response to pluton emplacement during arc-normal shortening (Saleeby, 1990; Paterson and Fowler, 1993; McNulty et al., 1996, 2000; Paterson and Miller, 1998; Paterson and Farris, 2008). At the largest scale, plutons emplaced at depths of as much as ~30 km and intruded into metamorphic strata only 1–5 m.y. older attest to downward transfer at rates of millimeters to centimeters per year that apparently occurs in response to tectonic and magmatic thickening of the lithospheric column (Saleeby, 1990; Paterson and Farris, 2008; Cao et al., 2016). Despite little subsequent testing of these conjectured tectonomagmatic links, these ideas have become widely influential.

Herein, we synthesize new and published geologic mapping, field observations, and zircon U-Pb geochronology from across the CSN to create an updated reconstruction of ~25 m.y. of extensively partitioned deformation that refines the timing and significance of mid-Cretaceous structural development. Comparing patterns of arc magmatism, intra-arc deformation, and orogenic evolution across the broader North American Cordilleran margin leads to a series of interrelated conclusions: (1) In contrast to previous models, magmatism and regional deformation show uncorrelated patterns in the mid-Cretaceous CSN across all scales of observation. (2) Regional deformation does not control the spatiotemporal patterns of magmatism nor vice versa. (3) Indirect tectonomagmatic links operate at multiple scales such that magmatic additions do not localize regional deformation within the arc and may instead rheologically strengthen arc lithosphere, partitioning deformation into the fore- and retro-arc. We conclude that orogen-scale tectonic interpretations must incorporate multiscale, non-steady-state deformation partitioning of far-field boundary conditions due to the structural impacts of arc activity as well as the evolution of lithospheric architecture. Consideration of these factors at scales ranging from individual magma pulses and shear zones to the entire lithospheric column and across-strike breadth of orogenic activity, in addition to plate-scale geodynamics, is needed to unravel the evolution of convergent margins.

METHODS

New geologic mapping at 1:5000 to 1:20,000 scales conducted during 2014–2020 focused on documenting field relationships, measuring structural data,

Downloaded from http://pubs.geoscienceworld.org/gsa/geosphere/article-pdf/18/6/1752/5737985/ges02478.1.pdf
by San Jose State Univ King Library Periodicals user

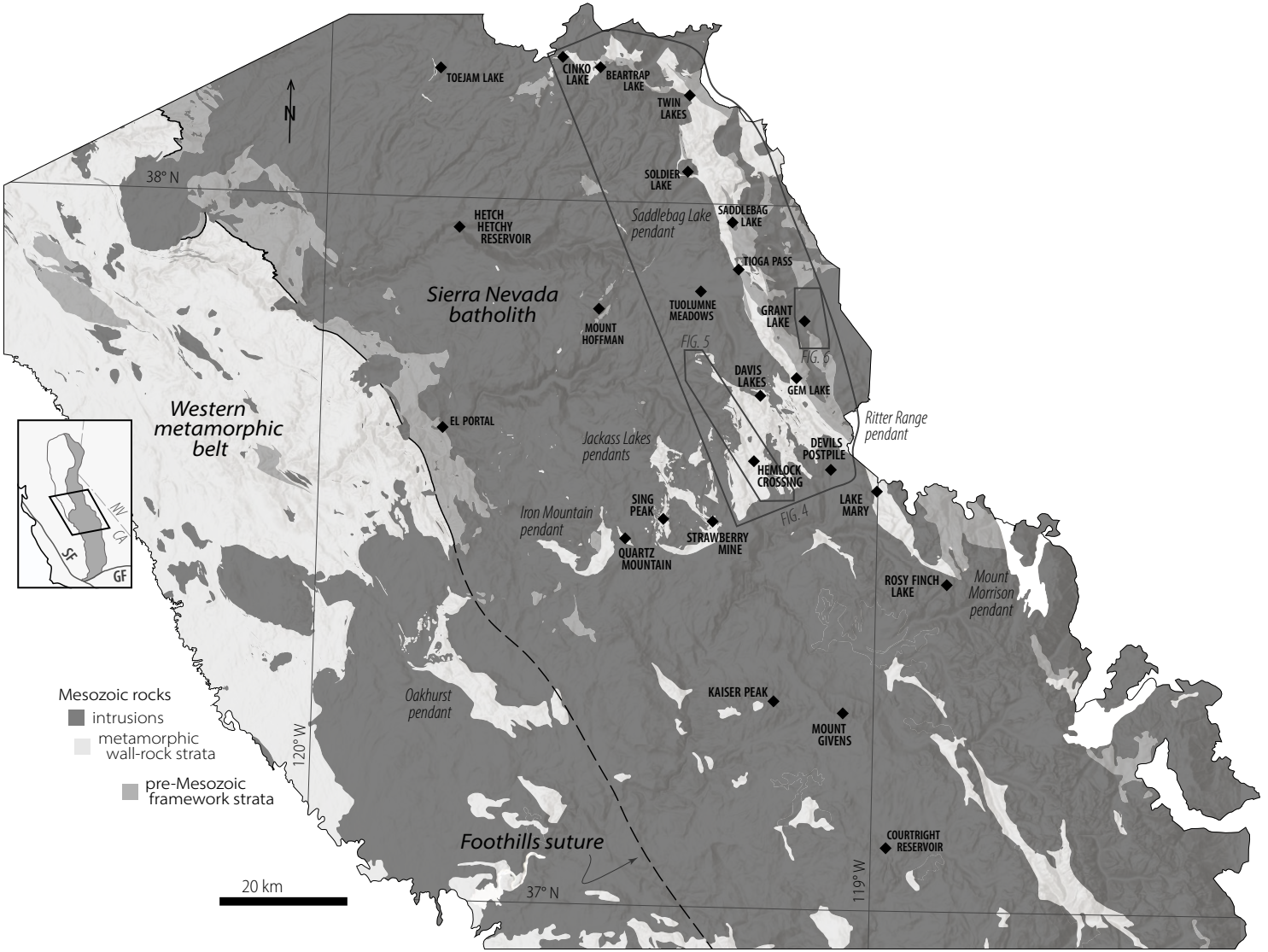

Figure 1. Geographic overview of the central Sierra Nevada, eastern California (USA), with simplified geology modified from Bateman (1992) and Jennings (2010). Latitude and longitude are in North American Datum of 1927. Inset map shows the position of the map area within the Sierra Nevada batholith (gray). CA—California; NV—Nevada; GF—Garlock fault; SF—San Andreas fault.

Downloaded from http://pubs.geoscienceworld.org/gsa/geosphere/article-pdf/18/6/1752/5737985/ges02478.1.pdf
by San Jose State Univ King Library Periodicals user

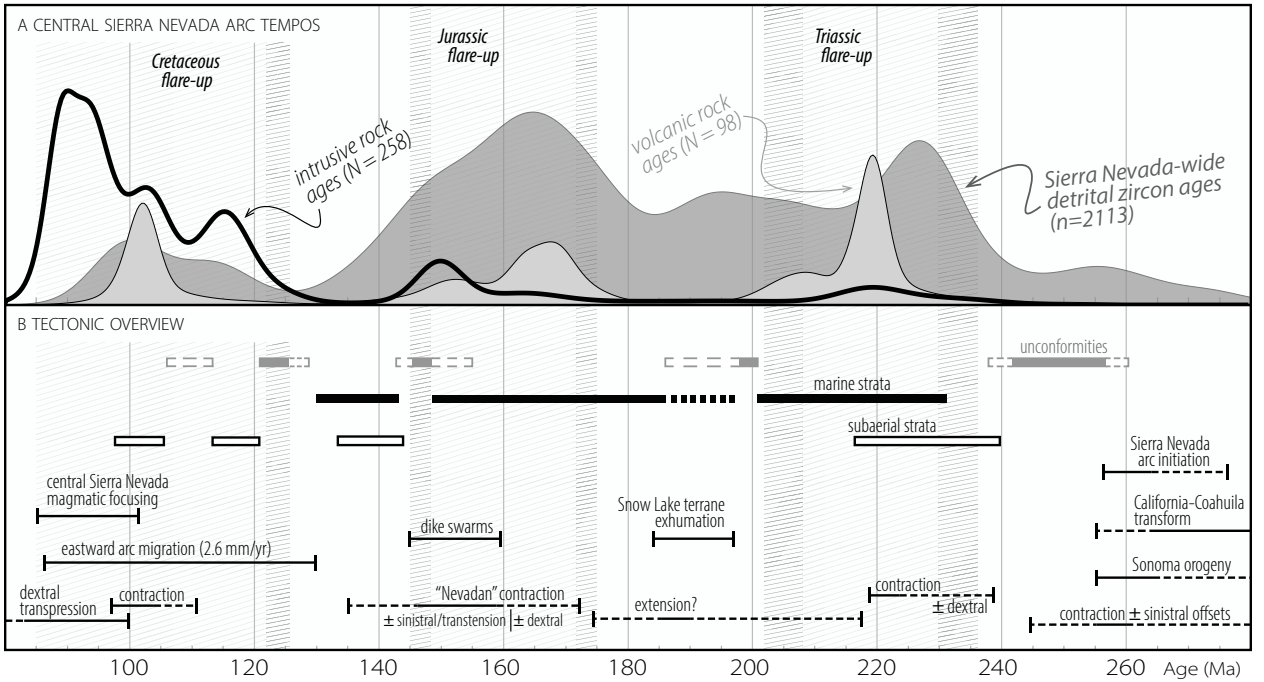

Figure 2. (A) Summary of central Sierra Nevada arc activity, showing relative probability density of compiled metavolcanic and plutonic rock ages as well as detrital zircon grain ages. (B) Sierra Nevada tectonostratigraphic development, with dashed intervals indicating uncertainty in age and local variations. Hachured intervals correspond to flare-up timing with more closely spaced hachured shoulders indicating uncertainty in age. Adapted from Attia et al. (2020, 2021) and references therein.

and collecting samples throughout the Ritter Range pendant and surrounding intrusions in the eastern-central Sierra Nevada (Fig. 1). New mapping in the eastern Ritter Range pendant focused on the structurally complex sequence of Triassic–Jurassic metamorphic strata and exposures of the Sierra Crest shear zone. Detailed mapping and field data collection also centered on the Bench Canyon shear zone in the western Ritter Range pendant. Further reconnaissance mapping was also conducted around the Reversed Peak shear zone, exposed in intrusions east of the Ritter Range pendant. New zircon U-Pb geochronology was conducted on 28 samples of intrusive and metavolcanic rocks from across the central Sierra Nevada (Fig. 3; Table 1) via laser ablation–inductively coupled mass spectrometry (LA-ICPMS) at the Arizona LaserChron Center (Tucson, Arizona, USA; Gehrels et al., 2006, 2008). Reduced isotopic age data were filtered prior to visualization and rock age calculation. Analyses younger than 500 Ma were excluded if the 2σ error ellipse did not intersect the concordia line. Rock ages were calculated as weighted mean ages with 95% confidence interval errors using Isoplot 3.75 (Ludwig, 2012). Complete analytical methods are given in File S1[1], analytical data as an EarthChem dataset[2], and rock age interpretations in File S3.

New and previously published zircon U-Pb geochronology data were compiled from across the CSN between ~37°N and 38.25°N. Data reduction and filtering choices differ across the compiled data set, and we thus follow the original given rock age interpretations. This compilation includes zircon U-Pb ages from 251 samples of Mesozoic plutons, 10 samples of Mesozoic hypabyssal intrusions, and 105 samples of Permo-Triassic to Cretaceous metavolcanic

[1]Supplemental Material. File S1: Geochronology analytical methods for LA-ICPMS analyses and geochronology compilation data sources. File S2: Data source information. File S3: Concordia plots and weighted mean age interpretations for new geochronology samples. File S4: Comprehensive details of the nature and age of central Sierra Nevada mid-Cretaceous structural features. Please visit https://doi.org/10.1130/GEOS.S.20443206 to access the supplemental material, and contact editing@geosociety.org with any questions.

[2]Complete data table, which contains isotopic ratios, dates, and uncertainties, is available through the EarthChem library: https://doi.org/10.26022/IEDA/111714.

Downloaded from http://pubs.geoscienceworld.org/gsa/geosphere/article-pdf/18/6/1752/5737985/ges02478.1.pdf
by San Jose State Univ King Library Periodicals user

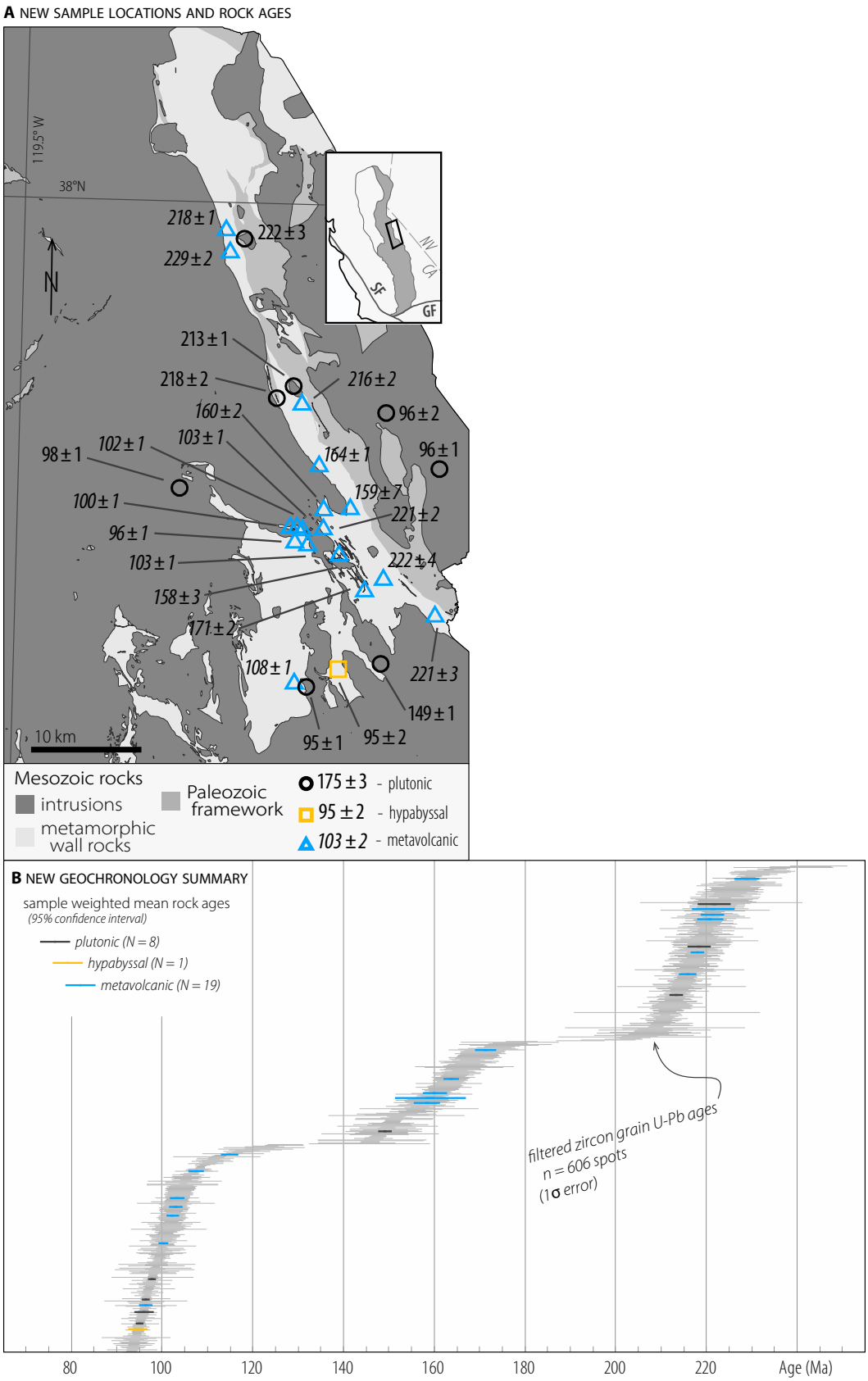

Figure 3. (A) Sample locations and rock ages (in Ma) for new geochronology analyses, given in Table 1, overlain on simplified geology of the eastern central Sierra Nevada. Sample FG-2-10 from west of the figure area is not shown here. CA—California; NV—Nevada; GF—Garlock fault; SF—San Andreas fault. (B) Summary of new zircon U-Pb geochronology data with individual analyses and uncertainties ordered by age rank and overlain by sample weighted mean ages and uncertainties.

Downloaded from http://pubs.geoscienceworld.org/gsa/geosphere/article-pdf/18/6/1752/5737985/ges02478.1.pdf
by San Jose State Univ King Library Periodicals user

TABLE 1. NEW GEOCHRONOLOGY SAMPLE SUMMARY

Sample name	Sample IGSN	Location*		Age† (Ma)	Unit
		Easting	Northing		
Metavolcanic strata					
A-145	IESNI001K	305022	4177889	96.4 ± 1.1	Ritter Range pendant
C-59	IESNI001M	304614	4178618	100.3 ± 0.8	"
DL16-26	IESNI001N	304925	4178608	102.3 ± 1.1	"
DL16-21	IESNI001O	305728	4177467	103.0 ± 1.2	"
DL16-88	IESNI001P	305428	4178548	103.3 ± 1.3	"
HC18-AW-13	IESNI001Q	304966	4164493	107.5 ± 1.3	"
D-142	IESNI001T	308873	4176416	158.4 ± 2.5	"
C-200	IESNI001U	309905	4180589	159.1 ± 6.9	"
B34A	IESNI001V	307496	4180488	160.1 ± 2.2	"
NR15-46	IESNI001W	307072	4184498	163.7 ± 1.4	"
VT15-22-B	IESNI0027	310447	4173520	N.D.§	"
VT16-11	IESNI001X	310881	4173460	171.3 ± 1.9	"
NR15-193	IESNI001Z	305385	4190532	215.9 ± 1.5	"
RR16-S-33	IESNI0022	317571	4170873	220.8 ± 2.5	"
A-71	IESNI0023	307317	4178774	221.3 ± 2.1	"
VT16-3-A	IESNI0024	312891	4174206	221.5 ± 4.0	"
1-19	IESNI0020	298662	4205876	218.0 ± 1.1	Saddlebag Lake pendant
3-93	IESNI0026	299023	4203864	228.9 ± 2.3	"
FG-2-10	IESNI001R	256840	4137312	114.9 ± 1.5	Oakhurst pendant
Hypabyssal intrusion					
HLA-51	IESNI001G	308919	4165862	94.7 ± 1.7	Ritter Range pendant
Plutons					
HC18-AW-17	IESNI001H	305900	4164272	95.1 ± 0.6	Mount Givens pluton
J17-568A	IESNI001I	312750	4188884	96.0 ± 1.8	Aeolian Buttes granodiorite
J17-567	IESNI001J	317971	4184010	96.4 ± 0.6	June Lake granite
BL18-1	IESNI001L	294425	4182310	97.7 ± 0.6	Red Devil Lake granodiorite
HL16-61	IESNI001S	312227	4166144	149.1 ± 1.2	Red Top Mountain granodiorite
NR16-1	IESNI001Y	304760	4191068	213.3 ± 1.2	Mono Pass granodiorite
NR15-188	IESNI0021	303247	4190438	218.4 ± 2.2	porphyritic granite dike
2-1	IESNI0025	300020	4205037	221.7 ± 3.2	Saddlebag Lake diorite

Note: IGSN—International GeoSample Sample Number. Quotation marks (") indicate ditto.
*Universal Transverse Mercator coordinates in meters given in North American Datum of 1927, zone 11.
†Uncertainty given is 95% confidence interval of weighted mean age.
§N.D.—no data; no reliable rock age estimate.

rocks as well as maximum depositional ages based on detrital zircon U-Pb age analyses of 31 samples of Neoproterozoic–Paleozoic metasedimentary strata and 50 samples of Permo-Triassic to Cretaceous metasedimentary strata. Fifteen plutonic, seven metavolcanic, and two metasedimentary samples with either no reliable rock age estimates or no location data are excluded from Figure 2A. A detailed listing of compiled data sources is given in File S1 (see footnote 1).

The geometry, characteristics, timing of development, and kinematics of structural features are synthesized from the new data presented herein and existing studies spanning the CSN. This synthesis includes fabrics and bedding in Cretaceous and older strata, magmatic foliations in Cretaceous intrusions, and mid-Cretaceous shear zones. Previous interpretations of structural features are reevaluated utilizing all available geochronology data and documented field relationships. Much of the published structural data are not available for reanalysis. Average structural orientations are the values given by previous studies except where attributed specifically to this study in reference to new measurements presented herein for the first time.

Downloaded from http://pubs.geoscienceworld.org/gsa/geosphere/article-pdf/18/6/1752/5737985/ges02478.1.pdf
by San Jose State Univ King Library Periodicals user

RESULTS

Geologic Mapping (Figures 5 and 6)

The Ritter Range pendant represents one of the largest contiguous exposures of metamorphic wall-rock strata in the Sierra Nevada (Fig. 1). Paleozoic and Mesozoic (ca. 222–202, 190–148, 107–97 Ma) metavolcanic and metasedimentary strata of the Ritter Range pendant are intruded by numerous Triassic, Jurassic, and Cretaceous (ca. 220–210, 168–149, 103–84 Ma) plutonic and hypabyssal intrusions (Fig. 4; Huber and Rinehart, 1965; Kistler, 1966; Tobisch et al., 1977, 2000; Attia et al., 2018, 2020, 2021; Barth et al., 2018). These intrusions provide many opportunities for dating crosscutting relationships that constrain the development timing of structural features, and the Ritter Range pendant thus preserves a rich record of Mesozoic deformation. Multiple phases of tectonism resulted in structurally repeated strata, steeply dipping bedding, development of single-phase cleavage and composite fabrics, brittle faulting, ductile shear, and sub-greenschist to amphibolite facies metamorphism (Schweickert et al., 1984; Paterson et al., 1989; Hanson et al., 1993; Sorensen et al., 1998). Although Ritter Range pendant wall-rock strata generally show steep to subvertical, SW-dipping bedding and subparallel penetrative foliations, mid-Cretaceous strata principally exposed in the axis of the pendant are only moderately to gently dipping (Tobisch et al., 1977; Fiske and Tobisch, 1978, 1994). The older, structurally repeated Triassic–Jurassic sequence provides metavolcanic rock ages and maximum depositional ages of interbedded metasedimentary strata as young as ca. 152–149 Ma. This is only marginally older, within uncertainty, than the ca. 149 Ma age of the Red Top Mountain pluton presented herein, which truncates these transposed strata (Fig. 4; Table 1). Given that this largely undeformed pluton was previously interpreted to be of Late Cretaceous age, this new date further supports that some significant deformation must have taken place in the Late Jurassic (e.g., Tobisch et al., 2000).

Hypabyssal intrusions dated to ca. 103–100 Ma crosscut penetrative foliations in both Triassic–Jurassic and Cretaceous strata across the Ritter Range pendant (Fig. 4; Tobisch et al., 2000; Attia et al., 2020). A solid-state foliation, broadly parallel to the composite cleavage in the surrounding Triassic–Jurassic strata, is developed locally within these latest Early Cretaceous hypabyssal intrusions and is itself truncated by ca. 95–93 Ma plutons (Sharp et al., 2000; Tobisch et al., 2000; Memeti et al., 2022). Moderately to steeply NW-dipping metavolcanic strata in the area around Davis Lakes are of uppermost Lower Cretaceous age (Figs. 1, 3, 4). Rock ages from this package range from ca. 103 to 101 Ma with one anomalous ca. 96 Ma age (Table 1), whereas crosscutting intrusions associated with the Tuolumne intrusive complex show ca. 95–93 Ma ages (Memeti et al., 2022). Penetrative foliations in mid-Cretaceous rocks, including metavolcanic strata and intrusions, indicate a component of mid-Cretaceous deformation (Tobisch et al., 2000). Foliations in Triassic–Jurassic strata of the eastern CSN are composite fabrics resulting from distinct mid-Cretaceous, Late Jurassic, and potentially Triassic tectonic episodes (Tobisch and Fiske, 1982).

Bench Canyon Shear Zone

The Bench Canyon shear zone is an ~2-km-wide, ~25-km-long, moderately to steeply WSW-dipping, reverse-sense shear zone best developed and exposed along the North Fork San Joaquin River in the western Ritter Range pendant (Fig. 4; McNulty, 1995). The Bench Canyon shear zone juxtaposed hanging-wall Upper Jurassic strata over Lower Cretaceous footwall strata (Fig. 5). The shear zone bifurcates to the north into the eastern Rodgers Peak thrust and the main western segment that deforms the ca. 98–95 Ma Red Devil Lake granodiorite. Both strands are truncated by the Tuolumne Intrusive Suite to the north, and the Mount Givens pluton truncates the shear zone to the south (Frazer et al., 2014). The core of the Bench Canyon shear zone is defined by mylonitic foliations dipping 56° toward 245° on average, nearly parallel transposed bedding, and an associated, well-developed stretching lineation that plunges just south of down-dip (Fig. 5). These mylonites give way to less-intense foliation developed in wall rocks to the east and west of the shear zone (Tobisch et al., 2000; Tomek et al., 2017). Strain analyses from within the Bench Canyon shear zone yield *Z*-axis shortening of ~60%–70%, with an estimated >5 km of thrust displacement (McNulty, 1995; Cao et al., 2016).

The Bench Canyon shear zone has been interpreted to record arc-normal horizontal contraction ca. 92–90 Ma with local brittle deformation possibly continuing to ca. 78 Ma (McNulty, 1995), but recently published geochronology of surrounding wall-rock strata and crosscutting intrusions (Frazer et al., 2014; Tomek et al., 2017; Attia et al., 2020), as well as new ages and mapping presented herein, require significant revision of shear-zone activity timing. Zircon U-Pb geochronology analyses of metavolcanic strata in the hanging wall of the main segment of the Bench Canyon shear zone previously interpreted as Lower Cretaceous yield ca. 158–149 Ma rock ages (Fig. 5). Metavolcanic strata in the footwall yield rock ages ca. 103–101 Ma. Although strata of the Minarets caldera generally dip gently to the southwest, bedding is increasingly deflected to steep dips subparallel to solid-state foliations approaching the shear zone (Tobisch et al., 2000). A package of footwall metavolcanic rocks near the southern terminus of the Bench Canyon shear zone that speculatively represent pre-caldera deposits yield a ca. 108 Ma rock age (Fig. 5; Table 1).

The ca. 101–100 Ma Shellenbarger Lake pluton (Fig. 5) truncates solid-state foliations developed in Minarets caldera strata but shows no subsequent solid-state fabrics, providing a minimum timing constraint on tilting and deformation of the Minarets caldera outside of the core of the Bench Canyon shear zone (Tomek et al., 2017). The Stevenson Meadow porphyritic gabbro intruded syn-kinematically into Minarets caldera strata along the periphery of the shear zone, where it truncates mylonitic fabrics in host rocks. The western portion of this intrusion experienced subsequent solid-state deformation, expressed as a disorganized network of millimeter-scale ductile-brittle shear bands (Fig. 5). Centimeter-scale feldspar lathes experienced both brittle and ductile deformation within these shear bands, indicative of progressive deformation under initially high temperatures. We assign this hypabyssal intrusion a tentative

Downloaded from http://pubs.geoscienceworld.org/gsa/geosphere/article-pdf/18/6/1752/5737985/ges02478.1.pdf
by San Jose State Univ King Library Periodicals user

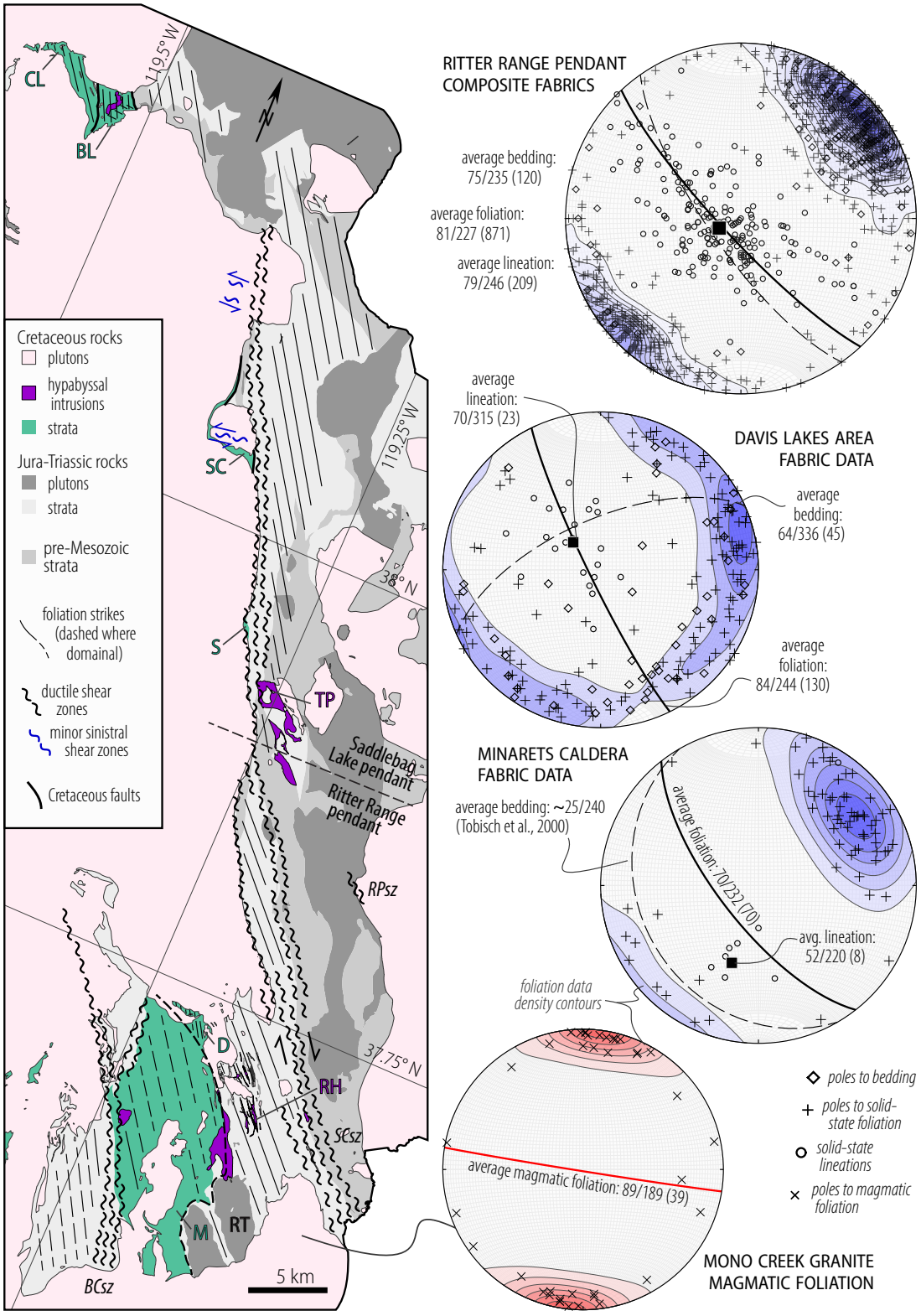

Figure 4. Simplified geology of the eastern central Sierra Nevada highlighting elements of mid-Cretaceous structural development. RT—Red Top Mountain pluton; other abbreviations as in Table 3. Geology modified from Huber and Rinehart (1965), Kistler (1966), Fiske and Tobisch (1978, 1994), Peck (1980), Bateman et al. (1983), Bateman (1992), Tobisch et al. (2000), Schweickert and Lahren (2006), Memeti et al. (2010a, 2010b, 2012), Cao et al. (2015), Cao (2016), Hartman et al. (2018), and Ardill et al. (2020a, 2020b). Latitude and longitude are in North American Datum of 1927. Structural measurements are given in dip and dip direction on stereonets, plotted using Stereonet 11 (Allmendinger et al., 2012; Cardozo and Allmendinger, 2013), with average orientations determined by Bingham eigenvector statistics and variable interval contours meant to qualitatively depict data density. Number of bedding, foliation, and lineation measurements plotted on each stereonet and used to calculate average orientations given in parentheses. Data in these stereonets are new and were collected in the field during mapping, except for the average bedding orientation provided for the Minarets caldera as given by Tobisch et al. (2000).

Downloaded from http://pubs.geoscienceworld.org/gsa/geosphere/article-pdf/18/6/1752/5737985/ges02478.1.pdf
by San Jose State Univ King Library Periodicals user

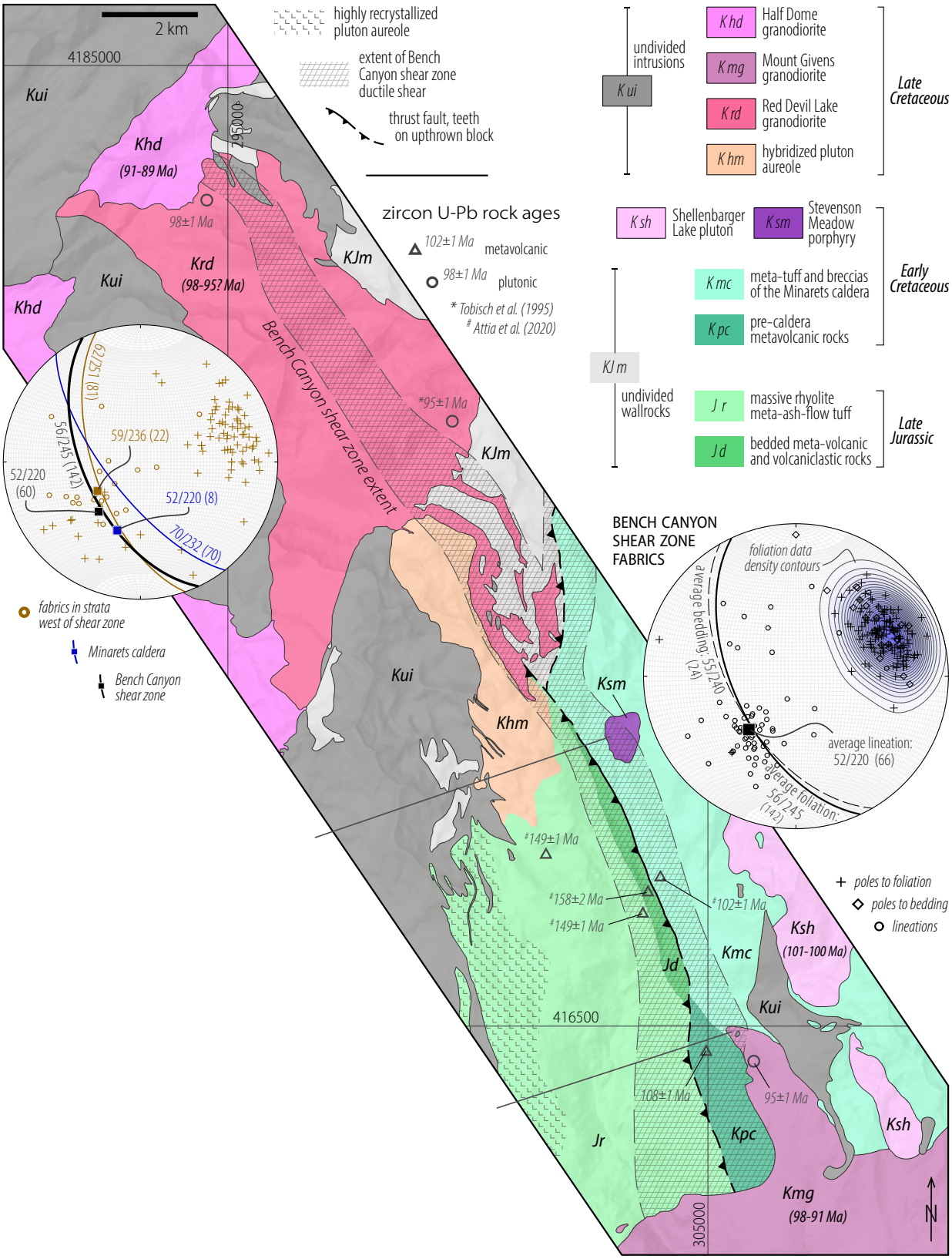

Figure 5. Bedrock geology of the Bench Canyon shear zone. Geology and ages are modified from Huber and Rinehart (1965), Peck (1980), Stern et al. (1981), Bateman et al. (1983), Fiske and Tobisch (1994), McNulty (1995), Memeti et al. (2010a), Frazer et al. (2014), Tomek et al. (2017), and Attia et al. (2020). Coordinates are Universal Transverse Mercator (in meters) in North American Datum of 1927, zone 11. New mapping presented herein focused on the central portion of the shear zone and surrounding metamorphic strata, south of the Red Devil Lake granodiorite. Structural measurements are given in dip and dip direction on stereonets. Number of measurements of each type plotted on the stereonets and used to calculate average orientations given in parentheses. All data given in these stereonets are new data collected in the field during mapping.

Downloaded from http://pubs.geoscienceworld.org/gsa/geosphere/article-pdf/18/6/1752/5737985/ges02478.1.pdf
by San Jose State Univ King Library Periodicals user

ca. 100 Ma age on the basis of correlations with similar hypabyssal intrusions in more eastern parts of the Ritter Range pendant.

The Bench Canyon shear zone is truncated at its southern terminus by the ca. 97–92 Ma northern lobe of the Mount Givens pluton, which is undeformed except for rare shear bands observed within a narrow finger of the Mount Givens pluton protruding to the northwest (Fig. 5; McNulty, 1995; Tobisch et al., 1995). New zircon U-Pb geochronology analyses from undeformed portions of this protrusion provide a ca. 95 Ma crystallization age (Table 1). Zircon U-Pb geochronology analyses of the Red Devil Lake granodiorite, deformed within the northern Bench Canyon shear zone, yield two ca. 98 Ma crystallization ages (Table 1; Stern et al., 1981) and one ca. 95 Ma crystallization age (Tobisch et al., 1995). We favor the ca. 98 Ma timing for intrusion of the Red Devil Lake granodiorite, which is consistent with the new analyses performed using modern methods presented herein, but cannot exclude the younger ca. 95 Ma age. Timing constraints and crosscutting relationships discussed above indicate that Bench Canyon shear zone reverse-sense motion initiated ca. 102–101 Ma at the latest. Initially widespread shear-zone deformation progressively localized onto the shear-zone core until the ca. 97–95 Ma cessation of shear. This is significantly older than the previously proposed ca. 92–90 Ma timing (cf. Tobisch et al., 1995; Nadin et al., 2016).

Reversed Peak Shear Zone

Kistler (1966) mapped and briefly described a zone of localized ductile deformation along the intrusive contact between the Late Cretaceous Aeolian Buttes granodiorite and the Triassic Lee Vining Canyon granite of the Scheelite Intrusive Suite, just east of the Sierra Nevada front (Figs. 4, 6). Bateman (1992) attributed this ductile shear to pluton emplacement processes. Hildreth et al. (2021) refuted previous models linking this shear zone with Quaternary volcanism in Mono Basin, a relatively low-relief area centered on Mono Lake to the northeast of Grant Lake, and speculated that it may be part of the larger dextral transpressional Sierra Crest shear zone system. This structure is herein named the Reversed Peak shear zone for excellent exposures along a prominent northwestern flank protruding from Reversed Peak toward the southeastern bank of Grant Lake (Figs. 1, 6). Unlike the high Sierra Nevada, this area sits in the hanging wall of range-bounding extensional frontal faults and may have experienced significant Cenozoic tilting. Preliminary mapping near Grant Lake reveals a NW-trending shear zone characterized by small-scale, ductile-brittle shear bands with variable orientations centered on a 1–10-m-scale band of subvertical mylonites developed within the Aeolian Buttes granodiorite (Fig. 6).

Mylonitic foliations in the center of the shear zone dip 88°SW on average with a down-dip, subvertical stretching lineation. Many millimeter- to meter-scale lenses of less-deformed plutonic material are enclosed within these mylonites. Minor subvertical to shallow-dipping, millimeter- to centimeter-scale shear bands with a wide range of orientations form disorganized networks on both sides of the core shear zone. Both stretching lineations and slickenlines developed on these ductile to brittle shear bands vary from down-dip to strike parallel with respect to shear planes (Fig. 6). The most localized of these small-scale shear bands consistently overprint the mylonitic foliation where they overlap, whereas shear bands with clearer ductile components in some cases coalesce into the mylonites. The June Lake granite appears to truncate this shear zone (Bateman, 1992).

One zircon U-Pb geochronology sample collected from the Aeolian Buttes granodiorite within the Reversed Peak shear zone just to the northwest of Grant Lake (sample J17-568A) provides a crystallization age of 96 ± 2 Ma (Table 1). A zircon U-Pb geochronology sample from the June Lake granite collected ~7 km southeast of Grant Lake (sample J17-567) provides a crystallization age of 96 ± 1 Ma (Table 1). These crystallization ages provide tight, significantly revised timing constraints on movement along the Reversed Peak shear zone, which was active by at least ca. 98 Ma and ceased by ca. 95 Ma at the latest. We cannot exclude the possibility that the Reversed Peak shear zone initiated prior to emplacement of the Aeolian Buttes granodiorite. Although the Reversed Peak shear zone is poorly characterized with no kinematic interpretation offered herein, it is significant as the furthest-inboard mid-Cretaceous shear zone identified in the CSN.

Geochronology Compilation

Zircon U-Pb rock ages of CSN Mesozoic intrusions show a major peak ca. 95–88 Ma and minor peaks ca. 150, 115, and 103 Ma, with subsidiary spreads ca. 235–210 Ma and ca. 170–155 Ma (Figs. 2A, 7; Table 2). This record is biased toward Cretaceous plutons, which comprise ~80% of compiled ages despite making up ~50%–55% of the aerial extent of the CSN. However, the proportion of Cretaceous plutons is much higher to the south or if the Western metamorphic belt (Fig. 1) is excluded. The distribution of all metavolcanic rock ages from across the entire CSN shows major peaks ca. 219, 170–165, and 102 Ma with minor peaks ca. 212–205 and 156–148 Ma (Fig. 2A).

STRUCTURAL SYNTHESIS

Magmatic Foliation

Voluminous intermediate to felsic plutons with crystallization ages spanning ca. 120–85 Ma dominate the CSN (Fig. 2; Bateman, 1992). These plutons preserve structures formed both below and above the magma solidus that record information about strain fields caused by magmatic processes as well as regional tectonics. We herein focus on the subset of magmatic fabrics thought to have tectonic significance: foliations and lineations defined by the alignment of primary magmatic mineral grains formed under melt-present conditions that *(1) transgress fabrics and internal boundaries related to pluton construction and (2) are generally consistent throughout individual plutons* (Paterson

Downloaded from http://pubs.geoscienceworld.org/gsa/geosphere/article-pdf/18/6/1752/5737985/ges02478.1.pdf
by San Jose State Univ King Library Periodicals user

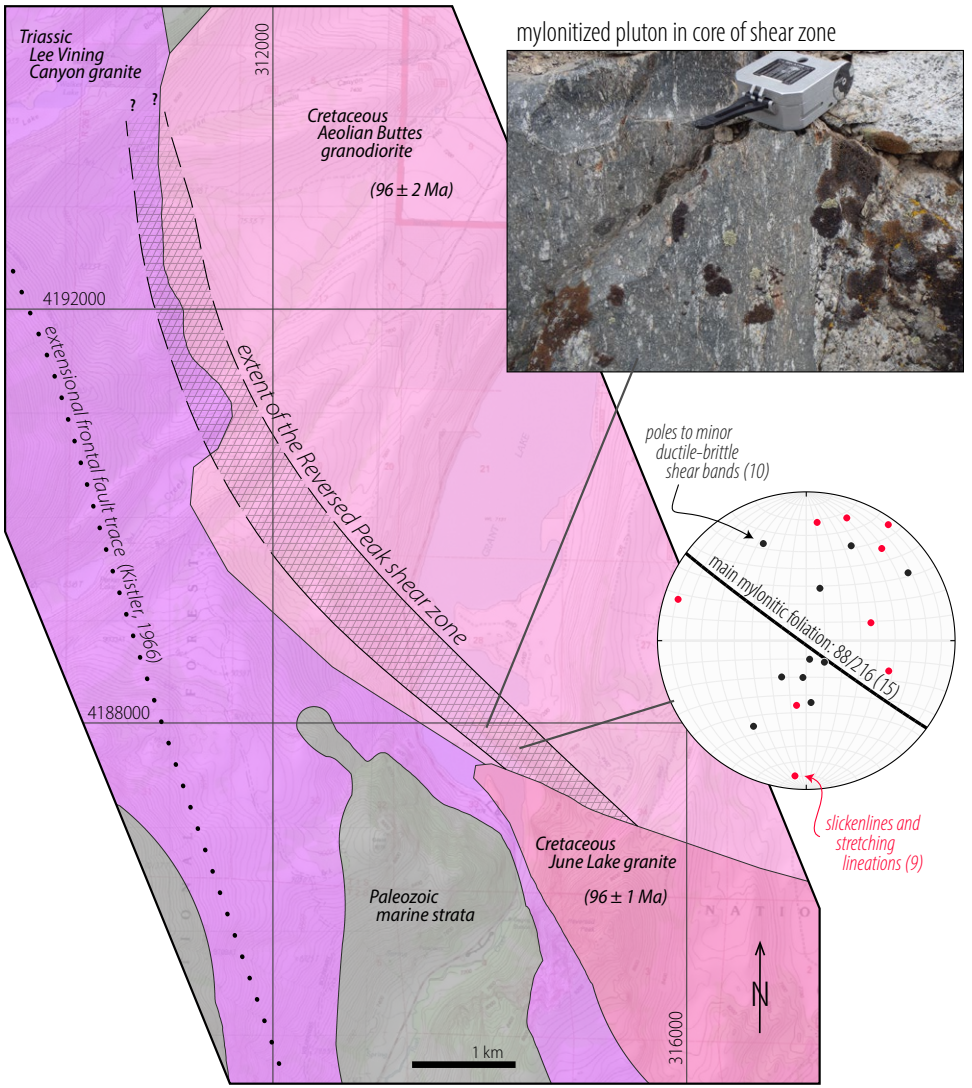

Figure 6. Bedrock geology of the Reversed Peak shear zone. Note that exposures of the shear zone lie in the hanging wall of Cenozoic extensional faults that bound the Sierra Nevada range front. Geology and ages are modified from Kistler (1966) and Bateman (1992), with new field observations focused on the southeastern end of the shear zone. Coordinates are Universal Transverse Mercator (in meters) in North American Datum of 1927, zone 11. Structural measurements are given in dip and dip direction on the stereonet. Number of measurements are given in dip and dip direction on stereonet and included in average given in parentheses. All data given in these stereonets are new data collected in the field during mapping.

Downloaded from http://pubs.geoscienceworld.org/gsa/geosphere/article-pdf/18/6/1752/5737985/ges02478.1.pdf
by San Jose State Univ King Library Periodicals user

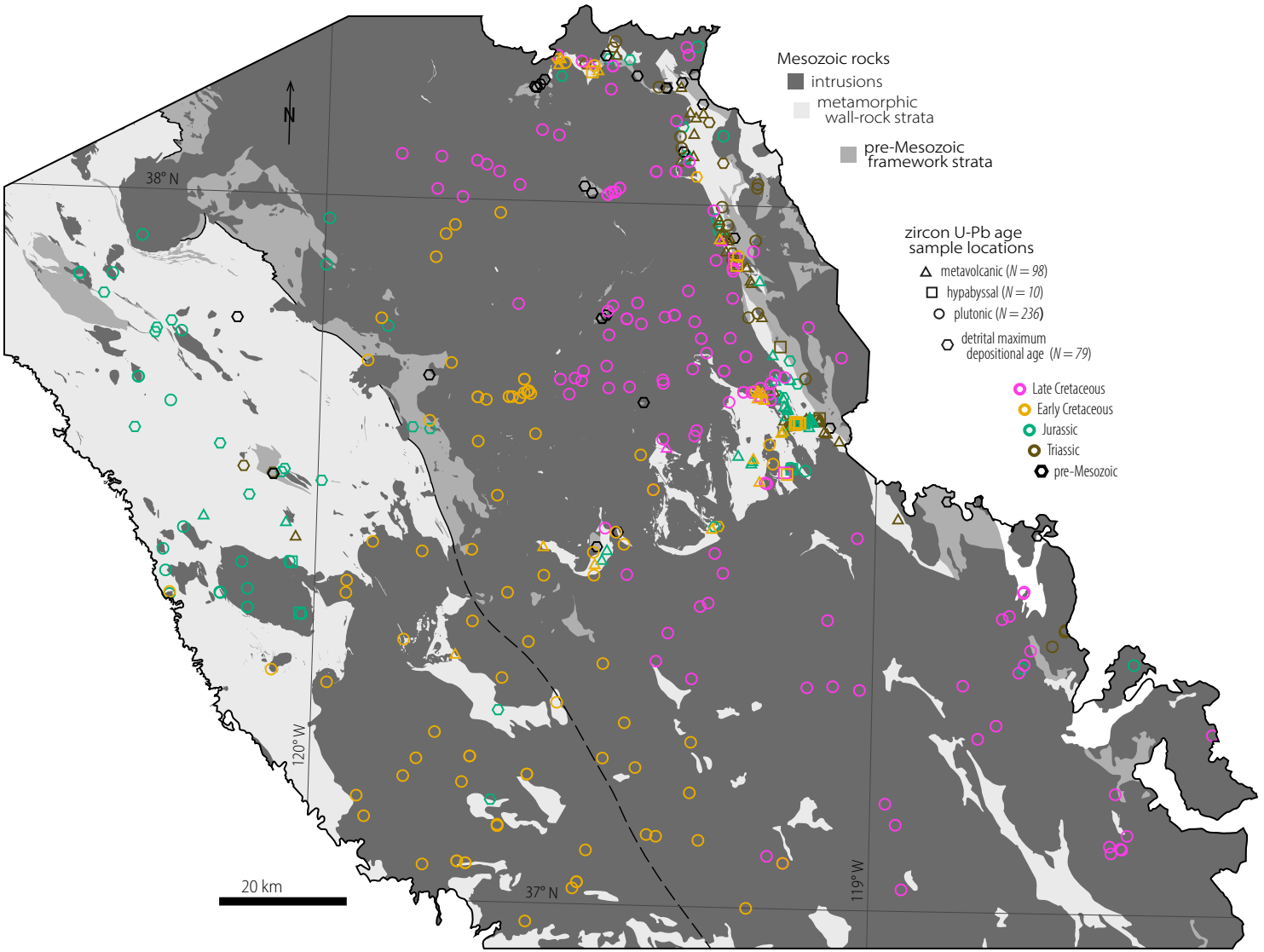

Figure 7. Summary map of compiled central Sierra Nevada zircon U-Pb rock ages, highlighting the eastward migration of mid-Cretaceous magmatism. Extent and geology are the same as in Figure 1. See File S1 (see text footnote 1) for data sources.

Downloaded from http://pubs.geoscienceworld.org/gsa/geosphere/article-pdf/18/6/1752/5737985/ges02478.1.pdf
by San Jose State Univ King Library Periodicals user

TABLE 2. CENTRAL SIERRA NEVADA ROCK AGE COMPILATION SUMMARY

Grouping	Age range (Ma)	*n*	References
Metamorphic wall-rock strata			
prebatholithic framework	Paleozoic	28	Grasse et al. (2001); Memeti et al. (2010b); Cao (2016); Attia et al. (2018, 2021); Ardill et al. (2020a)
Permo-Triassic	<255, 253	2	Attia et al. (2020, 2021)
Upper Triassic	232–202 (240*)	57	Tobisch et al. (2000); Barth et al. (2011, 2018); Cao et al. (2015); Cao (2016); Ardill et al. (2020a); Attia et al. (2020, 2021); this study
Lower Jurassic	195–180	12	Memeti et al. (2010b); Cao et al. (2015); Ardill et al. (2020a); Attia et al. (2020, 2021)
Middle–Upper Jurassic	174–148	61	Saleeby (1982); Tobisch et al. (2000); Snow and Ernst (2008); Barth et al. (2018); Attia et al. (2020, 2021); this study
Cretaceous	145, 135, 120–95	26	Stern et al. (1981); Memeti et al. (2010b); Cao et al. (2015); Cao (2016); Ardill (2020); Ardill et al. (2020a); Attia et al. (2020, 2021)
Intrusions			
Scheelite Intrusive Suite	235–213 (207,202)	15	Stern et al. (1981); Barth et al. (2011); Cao et al. (2015); Cao (2016); this study
Peñon Blanco assemblage	200–196, 190, 182	5	Stern et al. (1981); Saleeby (1982)
unassigned Jurassic plutons	180, 172–161, 150–146	18	Stern et al. (1981); Frost (1987); Saleeby et al. (1989); Tobisch et al. (2000); Nomade et al. (2003); Davis et al. (2012); Cao et al. (2015); Cao (2016); this study
Guadalupe igneous complex	149-148 (153–151)	10	Saleeby et al. (1989); Ernst et al. (2009); Ratschbacher et al. (2018)
unassigned Cretaceous plutons	138, 123, 120, 110, 101–93 (89)	24	Stern et al. (1981); Saleeby et al. (1989); Tobisch et al. (1995); Thompson et al. (2007); Cao et al. (2015); Leopold (2016); Tomek et al. (2017); Ardill et al. (2018, 2020a); Memeti et al. (2022); this study
Fine Gold Intrusive Suite	124–105	52	Stern et al. (1981); Dodge and Calk (1986); Lackey et al. (2012); Putnam et al. (2015)
Yosemite Valley intrusive suite	107–102 (110, 97, 96)	18	Stern et al. (1981); Ratajeski et al. (2001); Taylor (2004); Putnam et al. (2015); Ardill et al. (2018)
Buena Vista Crest intrusive suite	104–102 (112, 100, 99)	7	Stern et al. (1981); Tobisch et al. (1995); Putnam et al. (2015); Ardill et al. (2018)
Shaver Intrusive Suite	104–99 (123)	7	Stern et al. (1981); Tobisch et al. (1993); Lackey et al. (2012); Ardill et al. (2018)
Merced Peak intrusive suite	99–97 (107, 93)	5	Stern et al. (1981); McNulty et al. (1996)
Washburn Lake intrusive suite	98, 95	3	Stern et al. (1981); Tobisch et al. (1995); this study
Mount Givens pluton	98–90 (88)	18	Stern et al. (1981); Tobisch et al. (1993, 1995); Frazer et al. (2014); this study
Jack Main Canyon intrusive suite	98–95	8	Ardill et al. (2018); Scheland et al. (2018, 2019)
Yosemite Creek pluton	97	1	Burgess et al. (2009)
Sentinel pluton	95	2	Coleman and Glazner (1997); Burgess et al. (2009)
Sonora Pass intrusive suite	96, 90	2	Leopold (2016)
Tuolumne Intrusive Suite	95–84	37	Stern et al. (1981); Coleman and Glazner (1997); Coleman et al. (2004); Burgess and Miller (2008); Memeti et al. (2010b, 2022)
John Muir Intrusive Suite	96–84 (98, 76)	19	Stern et al. (1981); Frost and Mattinson (1988); Tobisch and Cruden (1995); Davis et al. (2012)
hypabyssal intrusions	232, 215, 105–95	2	Tobisch et al. (2000); Ardill et al. (2020a); Attia et al. (2020); this study

*Outliers are shown in parentheses; *n*—number.

et al., 1998, 2019; Vernon, 2000; Žák et al., 2007). These tectonically significant magmatic fabrics are not necessarily parallel to or directly continuous with solid-state fabrics in the surrounding wall rock. Because plutons crystallize quickly after emplacement, the orientations of such magmatic fabrics have been used to infer regional incremental strain at pluton crystallization ages (Berger and Pitcher, 1970; Ferré et al., 1995; Miller and Paterson, 1995; Petford et al., 2000; Benn et al., 2001; Callahan and Markley, 2003; Žák et al., 2007; Cao et al., 2015; Tomek et al., 2017). This strain increment corresponds to the transient period of melt-present yet crystal-rich conditions over which any magmatic foliations formed within each intrusion can be preserved.

Average orientations of internally throughgoing, time-transgressive (i.e., tectonically significant) magmatic foliations have been compiled from the 12 mid-Cretaceous intrusions and intrusive suites for which such data are available (Figs. 8, 9). These magmatic foliations show subvertical dips across the entire CSN. Based on compiled rock ages and field relationships, mid-Cretaceous CSN intrusions are herein grouped into three age ranges: ca. 106–99 Ma, 99–95 Ma, and 95–84 Ma. Compiled magmatic foliation orientations from coeval mid-Cretaceous plutons vary considerably on 10 km scales within each age group and are not always parallel to broadly coeval solid-state foliations (Fig. 9). Average trends of tectonically significant magmatic foliations vary

Downloaded from http://pubs.geoscienceworld.org/gsa/geosphere/article-pdf/18/6/1752/5737985/ges02478.1.pdf
by San Jose State Univ King Library Periodicals user

from NE-SW to WNW-ESE across intrusions within the 106–99 Ma group, from east-west to NNW-SSE within the 99–95 Ma group, and east-west to NNW-SSE within the 95–84 Ma group (Figs. 4, 8, 9; Table 3; McNulty et al., 1996; Taylor, 2004; Pignotta, 2006; McFarlan, 2007; Žak et al., 2007; Petsche, 2008; Yoshinobu et al., 2009; Pignotta et al., 2010; Paterson et al., 2011; Johnson, 2013; Van Dyne, 2014; Cao et al., 2015; Tomek et al., 2017; Scheland et al., 2018, 2019; Ardill et al., 2020a, 2020b). Cao et al. (2015) documented an apparent progressive rotation of magmatic foliations in ca. 98–85 Ma plutons in the Saddlebag Lake pendant (Fig. 1) from initial SSE-NNW trends toward east-west trends, which was interpreted to reflect rotation of regional incremental strain ellipsoid orientations due to progressively more-oblique subduction convergence. No such relationship between pluton age and orientation of tectonically significant magmatic foliation is observed at the scale of the entire arc segment.

Tilted Strata and Penetrative Foliation

In the CSN, penetrative fabrics outside of localized shear zones are principally developed in Paleozoic to Cretaceous metamorphic wall-rock strata. These ductile fabrics include composite foliations and lineations developed in pre-Cretaceous rocks, with mid-Cretaceous, Jurassic, and Triassic components, as well as single-phase fabrics in Cretaceous rocks formed during the mid-Cretaceous tectonic episode (Table 3; Tobisch et al., 2000). Cretaceous strata also experienced broadly coeval tilting (referring to horizontal-axis rotation throughout this paper). Penetrative fabric development and bedding rotation due to pluton emplacement–related stresses are only locally preserved, with nearly all observed deformation attributed to regional tectonism (cf. Bateman, 1992). Local bedding and cleavage deflection in Triassic–Jurassic strata of the Ritter Range pendant within <1 km of the Tuolumne intrusive complex have been attributed to pluton emplacement (Memeti et al., 2022). Rotation of bedding and pre-existing fabrics, as well as penetrative deformation and folding of dikes, during pluton construction have also been documented in pendants, screens, and stoped blocks associated with the Jackass Lakes pluton attributed to emplacement (Yoshinobu et al., 2009; Pignotta et al., 2010).

Triassic–Jurassic Strata

Triassic–Jurassic metamorphic wall-rock strata in the eastern CSN display variably striking, steep to vertical penetrative foliations that generally dip WSW with associated down-dip stretching lineations (Fig. 4; Table 3; Tobisch et al., 1977; Tobisch and Fiske, 1982; Cao et al., 2016). Tilting and penetrative deformation of pre-Cretaceous strata occurred during at least two tectonic episodes in the Jurassic and mid-Cretaceous (Tobisch et al., 2000). The composite nature of these fabrics is attested by truncation of tilted bedding and slaty cleavage in Triassic and Jurassic strata by Triassic–Jurassic plutons as well as the greater strain intensities observed in pre-Cretaceous rocks relative to mid-Cretaceous strata (Tobisch and Fiske, 1982; Cao et al., 2015). Mid-Cretaceous deformation of Triassic–Jurassic strata in the eastern CSN must have begun prior to the ca. 103–100 Ma emplacement of hypabyssal intrusions, which truncate bedding and foliation in both Triassic–Jurassic and Cretaceous strata. This phase of fabric development continued after the emplacement of hypabyssal intrusions that locally display weak solid-state fabrics and proceeded until the emplacement of the Tuolumne Intrusive Suite and associated plutons began ca. 95 Ma (Figs. 4, 8, 9). Thus, development of the younger component of these composite fabrics may have initiated any time after Late Jurassic pluton emplacement and may have continued locally until the ca. 82–80 Ma hornblende and biotite Ar-Ar cooling ages documented across the eastern CSN (Sharp et al., 2000; Cao, 2016). The variable observed, final orientations of these composite fabrics necessarily reflect the varied orientation of the overprinting mid-Cretaceous phase of fabric development.

Cretaceous Strata

Tilted and penetratively deformed Cretaceous strata represent a record of only Cretaceous deformation. The ages of crosscutting intrusions emplaced into deformed Cretaceous strata are consistent with tilting and fabric development ca. 103–96 Ma east of the Iron Mountain pendant (Figs. 1, 8, 9; Table 3; Ardill et al., 2020a). Due to uncertainties in the ages of some Cretaceous sequences and crosscutting intrusions, such deformation may have begun locally as early as ca. 117 Ma and continued until ca. 95 Ma (Cao et al., 2015). Cretaceous strata in the axial to eastern CSN display bedding with dips that vary from gentle to subvertical and strikes that vary from NNW to SW and SE on 1–10 km scales (Fig. 9; Table 3; Fiske and Tobisch, 1994; Cao, 2016; Tomek et al., 2017; Hartman et al., 2018). There is no apparent relationship between the dip or strike of tilted bedding in mid-Cretaceous strata and the constrained timing during which deformation occurred in each package. Foliations in mid-Cretaceous strata, necessarily reflecting only a single Cretaceous deformation phase, are generally steep to subvertical and strike NW to NNW or SE to SSE (Figs. 4, 9; Table 3).

Hypabyssal Intrusions

Mid-Cretaceous hypabyssal intrusions, interpreted as subvolcanic features emplaced at shallow levels, are found in Paleozoic and Triassic–Cretaceous strata across the eastern CSN (Tobisch et al., 2000; Cao, 2016; Ardill et al., 2018, 2020a). Such hypabyssal intrusions are found across the entire Ritter Range pendant with map view geometries that vary from nearly circular to tabular bodies oriented parallel to subparallel to the regional NNW tectonic grain (Fig. 4). These subvolcanic units vary in composition from basaltic to rhyolitic and in texture from aphanitic to porphyritic to clastic (Huber and Rinehart, 1965; Tobisch et al., 2000; Ardill et al., 2018). Notable examples include

Downloaded from http://pubs.geoscienceworld.org/gsa/geosphere/article-pdf/18/6/1752/5737985/ges02478.1.pdf
by San Jose State Univ King Library Periodicals user

the Stevenson Meadow porphyritic gabbro intruding into the Bench Canyon shear zone, an intrusive breccia complex and associated bimodal dikes and sills in the central Ritter Range pendant, and a large andesitic intrusion with variable textures built across the boundary between Lower Cretaceous strata and Triassic–Jurassic strata just east of the Minarets caldera (Figs. 4, 5; Fiske and Tobisch, 1978). The presence of high volumes of clastic material, pumiceous fragments, miarolitic cavities, and vesicular textures may indicate emplacement as subvolcanic fissures near the earth's surface (Nakamura, 1977; Tobisch et al., 2000). Eight zircon U-Pb geochronology analyses from Ritter Range pendant hypabyssal intrusions provide rock ages of ca. 103–100 Ma (Fig. 7; Tobisch et al., 2000; Attia et al., 2020). Locally, these hypabyssal intrusions are truncated by ca. 95–93 Ma granodiorites emanating southward from the Tuolumne Intrusive Suite (Tobisch et al., 2000; Memeti et al., 2022). The ca. 100 Ma Tioga Pass and Beartrap Lake hypabyssal complexes are prominent examples of such features in the Saddlebag Lake pendant (Cao, 2016; Ardill et al., 2020a).

These hypabyssal intrusions serve as structural markers that establish several key field relationships. Hypabyssal intrusions truncate tilted bedding and penetrative cleavage in surrounding wall rocks and are found within mid-Cretaceous shear zones as well as their country rocks (Figs. 4, 5). These

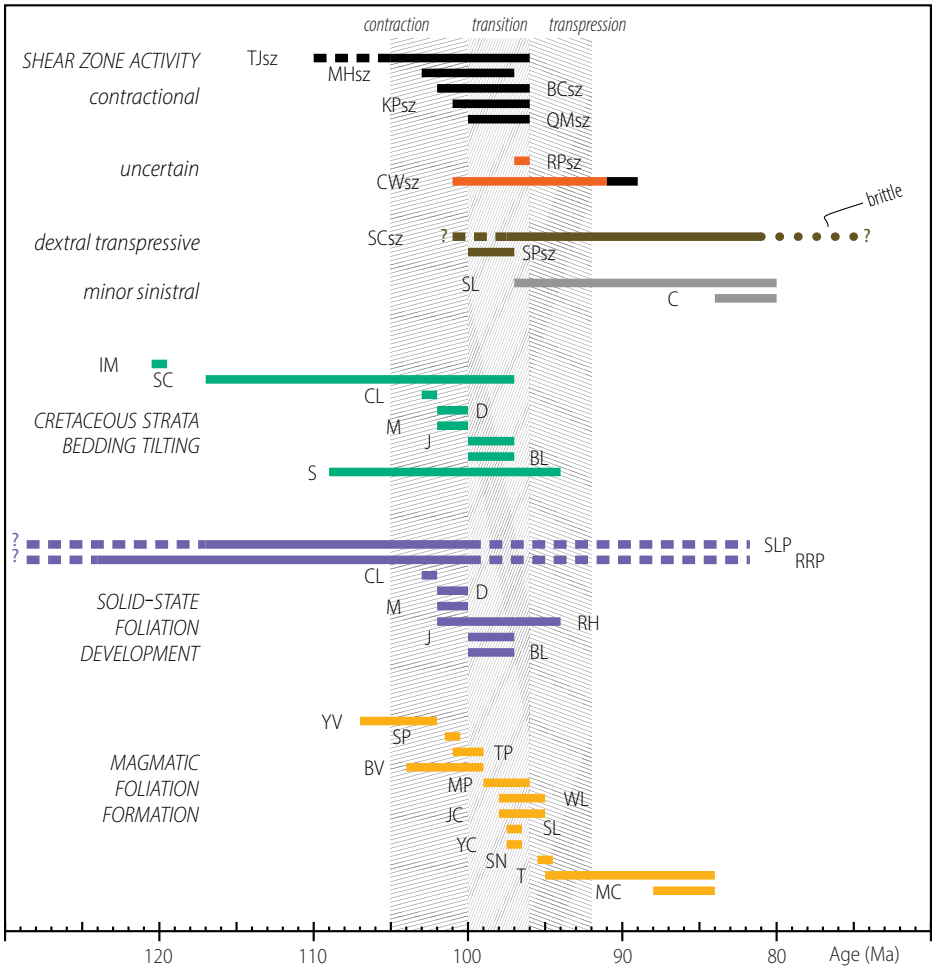

Figure 8. Summary of initiation and cessation timing of mid-Cretaceous structural features in the central Sierra Nevada. Dashed lines indicate uncertainty in timing constraints. Minor sinistral shears associated with the northern Sierra Crest shear zone in the Cathedral Peak granite (C) and Soldier Lake pluton (SL) are interpreted as subsidiary structures. All other abbreviations are as in Table 3.

Downloaded from http://pubs.geoscienceworld.org/gsa/geosphere/article-pdf/18/6/1752/5737985/ges02478.1.pdf
by San Jose State Univ King Library Periodicals user

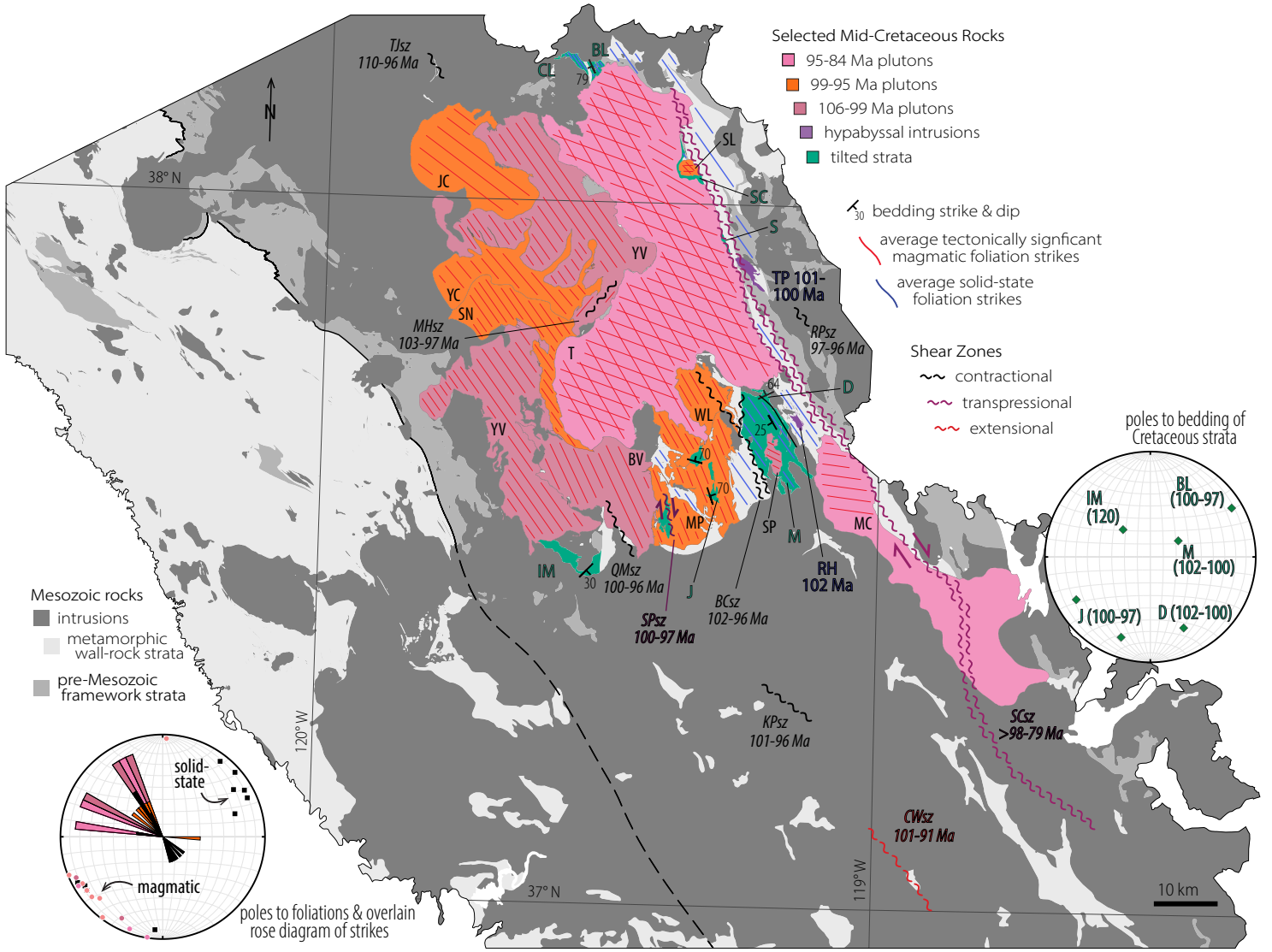

Figure 9. Summary of spatiotemporal trends of deformation during the mid-Cretaceous orogenic episode in the central Sierra Nevada. Varied orientations and degree of tilting of Cretaceous strata, shown as green diamonds in the right stereonet labeled with timing of tilting in Ma, indicate heterogeneous shortening directions and strain intensities, respectively. Persistently variable strikes of magmatic foliations across all mid-Cretaceous pluton age groups correspond to the averages summarized in Table 3 and are also shown as a color-coded rose diagram in the left stereonet. Only intrusions with available structural data are highlighted in color; see Ardill et al. (2020b) for details of Tuolumne Intrusive Suite fabrics. Stereonets show average orientations of structural feature sets as given in Table 3. Extent is the same as in Figure 1. Abbreviations are the same as in Figure 8 and Table 3.

Downloaded from http://pubs.geoscienceworld.org/gsa/geosphere/article-pdf/18/6/1752/5737985/ges02478.1.pdf
by San Jose State Univ King Library Periodicals user

intrusions locally display post-emplacement solid-state foliations (Tobisch and Fiske, 1982; Tobisch et al., 2000; Cao, 2016), with more intense deformation where they were emplaced within shear zones. Some of these intrusions are NNW-trending, steep to vertical sills and dikes and therefore accommodated very minor horizontal dilation (<1%) subparallel to coeval regional maximum shortening directions. Hypabyssal bodies intrude mid-Cretaceous metamorphic strata that were originally deposited at the earth's surface, both of which were subsequently intruded by plutonic rocks emplaced at a depth of ~6–10 km (Memeti et al., 2022). Thus, these features record progressive downward transfer from the earth's surface to hypabyssal emplacement depths and then to plutonic emplacement depths.

Shear Zones

Figure 8 summarizes the timing of mid-Cretaceous CSN shear zones, with field relationships and orientations shown on Figure 9. These shear zones show variable strikes from SE-NW to NE-SW, dominated by NNW-SSE trends parallel to the structural grain of the Sierra Nevada, and variable kinematics from reverse sense to dextral transpression to sinistral strike-slip and even a single shear zone with interpreted normal-sense motion (Figs. 4–6, 9). Mid-Cretaceous ductile shear zones in the axial to eastern CSN were active from as early as ca. 110 Ma to ca. 80 Ma, but the timing of activity along individual shear zones varies significantly. The spatiotemporal patterns of mid-Cretaceous shear-zone activity established herein differ significantly from previously proposed models.

Reverse-Sense Kinematics

Mid-Cretaceous shear zones with reverse-sense kinematics developed in both intrusive and metamorphic rocks (Figs. 5, 9; Table 3; Tobisch et al., 1993, 1995; Tong, 1994; McNulty, 1995; Johnson, 2013; Van Dyne, 2014; Leopold, 2016). These structures are defined by zones as much as several kilometers wide and as much as tens of kilometers long of steep to vertical penetrative foliations and discrete mylonitic to ultramylonitic shears with approximately down-dip stretching lineations. Most shear zones show NNW-SSE trends but can vary in strike by as much as ~30° between shear zones (Fig. 9). The Mount Hoffman shear zone is a notable outlier that strikes NE-SW (Johnson, 2013). Ages of pre-, syn-, and post-kinematic intrusions indicate that these shear zones were possibly active as early as ca. 110 Ma and as late as ca. 96 Ma, with no apparent trends in timing with respect to their position along and across strike of the arc (Figs. 8, 9; Table 3).

The amount of contraction that these reverse-sense shear zones accommodated is unclear due to their steep to subvertical dips, which would limit the horizontal shortening resulting from any motion along the shear plane. Either (1) these structures have been steepened from their original dips by progressive deformation or (2) they initially formed at such presently high dips and mostly accommodated relative vertical motions between their hanging walls and footwalls with little significant heave component. Widespread penetrative fabric development coeval with shear-zone activity (Fig. 9; Table 3) as well as observations of conjugate sets of mylonitic shears from the Kaiser Peak and Quartz Mountain shear zones that appear to have been progressively steepened are indicative of progressive horizontal shortening during mid-Cretaceous tectonism (Tobisch et al., 1995). Thus, we favor the interpretation that mylonitic foliations within these reverse-sense shear zones were steepened during progressive deformation. Strain analyses indicate ~60%–70% *Z*-axis shortening and multi-kilometer-scale thrust displacement in the Bench Canyon shear zone (McNulty, 1995). Similar shortening estimates are indicated by strain analyses from other CSN reverse-sense shear zones (Tobisch et al., 1993; Tong, 1994).

Dextral Transpressional Kinematics

Late Cretaceous, NNW-trending shear zones interpreted to have accommodated dextral transpression ca. 100–80 Ma are also found in the axial to eastern CSN (Fig. 9; Greene and Schweickert, 1995; Tikoff and Greene, 1997; Tikoff et al., 2005; Jiang and Bentley, 2012; Nadin et al., 2016; Krueger and Yoshinobu, 2018). The Sing Peak shear zone is defined by steep to subvertical, mylonitic to magmatic foliations developed in Jurassic and Cretaceous host rocks and the intruding ca. 99–97 Ma Jackass Lakes pluton in the axial CSN (Fig. 9; Krueger and Yoshinobu, 2018). Activity along the Sing Peak shear zone is constrained to ca. 100–97 Ma (Fig. 8; Stern et al., 1981; McNulty et al., 1996; Memeti et al., 2010b). The Sierra Crest shear zone system is a series of dextral transpressional shear zones defined by subvertical mylonites exposed along the easternmost CSN (Fig. 9; Tikoff and Greene, 1997). Although previously treated as a set of related but distinct shear zones (Greene and Schweickert, 1995; Tikoff and Greene, 1997; Tikoff et al., 2005; Horsman et al., 2008; Nadin et al., 2016), the northern portion of this system forms a single continuous shear zone that is variably intruded by Late Cretaceous plutons from the southernmost Ritter Range pendant to its terminus in the northern Saddlebag Lake pendant (Fig. 4; Cao, 2016).

The northern Sierra Crest shear zone consists of multiple anastomosing, narrow, simple shear–dominated strands with triclinic fabric symmetry that are separated by broad, lenticular, pure shear–dominated domains characterized by transposition of older fabrics, kinematic indicators with inconsistent shear sense, and symmetric chocolate-tablet boudinage and folds (Greene and Schweickert, 1995; Jiang and Bentley, 2012). Mineral lineations display orientations varying from down-dip to horizontal, defining a full girdle along the transposition foliation (Jiang, 2014). Recently published pluton crystallization ages show that ductile shear along the Saddlebag Lake portion of the northern Sierra Crest shear zone initiated prior to ca. 98 Ma and continued until a ca. 82–80 Ma transition to a localized, brittle fault system that was superposed onto the preceding mylonites (Cao et al., 2015; Hartman et al., 2018; Ardill et al., 2020a). Geochronology from the Ritter Range pendant

Downloaded from http://pubs.geoscienceworld.org/gsa/geosphere/article-pdf/18/6/1752/5737985/ges02478.1.pdf
by San Jose State Univ King Library Periodicals user

TABLE 3. CENTRAL SIERRA NEVADA MID-CRETACEOUS STRUCTURAL SUMMARY

Feature name (abbreviation)	Dip (degrees)	Strike or trend (degrees)	Timing (Ma)		Reference
			Maximum	Minimum	
Contractional shear zones					
Toejam Lake (TJsz)	Steep	SSE	110	96	Leopold (2016)
Mount Hoffman (MHsz)	Steep	NE	103	97	Burgess et al. (2009); Johnson (2013); Van Dyne (2014)
Bench Canyon (BCsz)	56	155	102	96	McNulty (1995); Tobisch et al. (1995); Frazer et al. (2014); this study
Kaiser Peak (KPsz)	Steep	NW	101	96	Tobisch et al. (1995)
Quartz Mountain (QMsz)	Steep	NNW	100	96	Tong (1994); Tobisch et al. (1995); Frazer et al. (2014)
Late Courtright-Wishon (CWsz) shortening	Vertical	NNW	91	89	Tobisch et al. (1993, 1995)
Shear zones with uncertain kinematics					
Courtright-Wishon (CWsz)	Steep	SSE	101	91	Renne et al. (1993); Tobisch et al. (1993, 1995)
Reversed Peak (RPsz)	88	126	97	96	Kistler (1966); Bateman (1992); Hildreth et al. (2021); this study
Dextral transpressional shear zones					
Sing Peak (SPsz)	Steep to vertical	NNW	100	97	Krueger and Yoshinobu (2018)
Northern Sierra Crest (SCsz), ductile	Steep to vertical	NNW	>98	81	Greene and Schweickert (1995); Tikoff and Greene (1997); Bentley (2004); Tikoff et al. (2005); Jiang and Bentley (2012); Jiang (2014); Cao et al. (2015); Ardill et al. (2020a); Memeti et al. (2022); this study
Northern Sierra Crest (SCsz), brittle	Steep to vertical	NNW	81	<79	Tobisch et al. (1995); Sharp et al. (2000); Pachell and Evans (2002); Compton et al. (2017); Hartman et al. (2018); this study
Tilted Cretaceous strata					
Iron Mountain pendant (IM)	~30	~045	120	120	Ardill et al. (2018); Ardill (2020)
Spiller Canyon area (SC)	Steep to vertical	NW	117	97	Mundil et al. (2004); Cao et al. (2015)
Cinko Lake area (CL)	Steep to vertical	NW	103	102	Memeti et al. (2010b); Cao (2016)
Davis Lakes area (D)	64	246	102	100	Attia et al. (2020); Memeti et al. (2022); this study
Minarets caldera (M)	~25	~150	102	100	Tobisch and Fiske (1982); Fiske and Tobisch (1994); McNulty (1995); Tobisch et al. (2000); Tomek et al. (2017); this study
Jackass Lakes pendants (J)	~70	NNW and WNW	100	97	Stern et al. (1981); McNulty et al. (1996); Yoshinobu et al. (2009); Memeti et al. (2010b); Pignotta et al. (2010); Krueger and Yoshinobu (2018)
Beartrap Lake area (BL)	79	149	100	97	Cao (2016)
Sawmill Canyon area (S)	Steep	NNW	109	94	Cao et al. (2015); Paterson et al. (2016); Hartman et al. (2018); Ardill et al. (2020a)
Solid-state foliations					
Saddlebag Lake pendant (SLP)	79	328	<154	81	Cao et al. (2015, 2016); Attia et al. (2021)
Ritter Range pendant (RRP)	81	137	<148	81	Tobisch and Fiske (1982); Sharp et al. (2000); Tobisch et al. (2000); Attia et al. (2020, 2021); this study
Cinko Lake area (CL)	84	321	103	102	Memeti et al. (2010b); Paterson et al. (2014); Cao et al. (2016)
Davis Lakes area (D)	84	154	101	100	Tomek et al. (2017); Memeti et al. (2022)
Minarets caldera (M)	70	142	101	100	Tobisch and Fiske (1982); Tomek et al. (2017); this study
Ritter Range pendant hypabyssal intrusions (RH)	88	133	102	94	Tobisch et al. (2000); Attia et al. (2020); Memeti et al. (2022); this study
Jackass Lakes pendants (J)	85	333	100	97	Stern et al. (1981); McNulty et al. (1996); Yoshinobu et al. (2009); Memeti et al. (2010b); Pignotta et al. (2010); Krueger and Yoshinobu (2018)
Beartrap Lake area (BL)	85	155	100	97	Cao (2016)

(*continued*)

Downloaded from http://pubs.geoscienceworld.org/gsa/geosphere/article-pdf/18/6/1752/5737985/ges02478.1.pdf
by San Jose State Univ King Library Periodicals user

TABLE 3. CENTRAL SIERRA NEVADA MID-CRETACEOUS STRUCTURAL SUMMARY (*continued*)

Feature name (abbreviation)	Dip (degrees)	Strike or trend (degrees)	Timing (Ma)		Reference
			Maximum	Minimum	
Magmatic foliations					
Yosemite Valley intrusive suite (YV)	80	325 and 040	107	102	Stern et al. (1981); Ratajeski et al. (2001); Taylor (2004); McFarlan (2007); Johnson (2013); Van Dyne (2014); Putnam et al. (2015); Ardill et al. (2018); Scheland et al. (2018, 2019)
Buena Vista Crest intrusive suite (BV)	83	335	104	99	Stern et al. (1981); Tobisch et al. (1995); McFarlan (2007); Putnam et al. (2015); Ardill et al. (2018)
Shellenbarger pluton (SP)	78	297	101	100	Fiske and Tobisch (1994); McNulty (1995); Tomek et al. (2017)
Tioga Pass hypabyssal complex (TP)	83	147	101	99	Ardill et al. (2020a)
Merced Peak intrusive suite (MP)	89	338	99	96	Stern et al. (1981); Tobisch et al. (1995); McNulty et al. (1996); Yoshinobu et al. (2009); Pignotta et al. (2010); Frazer et al. (2014); Krueger and Yoshinobu (2018)
Washburn Lake intrusive suite (WL)	Steep to vertical	~330	98	95	Peck (1980); Stern et al. (1981); Tobisch et al. (1995); Pignotta et al. (2010)
Jack Main Canyon intrusive suite (JC)	88	307	98	95	Ardill et al. (2018); Scheland et al. (2018, 2019)
Soldier Lake pluton (SL), NNW foliation	75	316	97	97	Mundil et al. (2004); Cao et al. (2015)
Soldier Lake pluton (SL), east-west foliation	86	92	97	97	Ibid.
Yosemite Creek pluton (YC)	Steep to vertical	~320	97	97	Burgess et al. (2009); Johnson (2013); Van Dyne (2014)
Sentinel pluton (SN)	Steep to vertical	~325	95	95	Coleman and Glazner (1997); Petsche (2008); Burgess et al. (2009)
Tuolumne Intrusive Suite (T), NNW foliation	Subvertical	~330	95	84	Stern et al. (1981); Coleman and Glazner (1997); Coleman et al. (2004); Žak et al. (2007); Burgess and Miller (2008); Memeti et al. (2010a); Paterson et al. (2011, 2016); Cao et al. (2015); Ardill et al. (2020b); Chambers et al. (2020); Memeti et al. (2022)
Tuolumne Intrusive Suite (T), east-west foliation	Subvertical	~290	95	84	Ibid.
Mono Creek granite (MC)	89	099	88	84	Stern et al. (1981); Davis et al. (2012); this study

Note: Detailed structural and age synthesis is given in Supplemental File S4 (see text footnote 1).

indicates that the northern Sierra Crest shear zone also initiated there prior to ca. 98 Ma, continuing until ca. 82–80 Ma (Fig. 4; Sharp et al., 2000; Bentley, 2004; Memeti et al., 2022).

Uncertain Kinematics

Two CSN shear zones active in the mid-Cretaceous, the Reversed Peak and Courtright-Wishon shear zones, have poorly constrained kinematics. Despite this, the Reversed Peak shear zone is still significant as the furthest-inboard ductile shear zone yet recognized in the CSN (Fig. 9). The Courtright-Wishon shear zone is an ~1-km-wide zone of steep to subvertical, NNW-trending cleavage and mylonitic to ultramylonitic foliations extending >10 km along the southwestern margin of the Mount Givens pluton. It was previously interpreted to display west-side-down, normal-sense motion ca. 101–91 Ma, followed by superposed horizontal shortening ca. 90 Ma (Fig. 9; Bateman et al., 1984; Tobisch et al., 1993, 1995). The normal-sense kinematics of the Courtright-Wishon shear zone is unique among mid-Cretaceous CSN shear zones, and this interpretation is open to debate due to contradictory field relationships, its subvertical to vertical dip, and limited study. The significance of the Courtright-Wishon shear zone for tectonic models is unclear given such ambiguity.

DISCUSSION

Tectonic Synthesis

Heterogeneous deformation is ubiquitous at all scales of observation throughout the mid-Cretaceous orogenic episode. This complexity at mid-upper crustal levels mirrors the tectonic complexity observed in active arcs (Kokkalas and Aydin, 2013; Stanton-Yonge et al., 2016). At the largest scale, adjacent 10–100-km-scale domains exhibit unique structural development. The western portion of the CSN, from the Iron Mountain pendant to the west, shows no significant ca. 110–80 Ma ductile deformation. In contrast, from east of the Iron Mountain pendant to at least as far east as Grant Lake, the axial to eastern portion of the CSN experienced intense deformation at this time (Fig. 9). Mid-Cretaceous tectonic and magmatic activity were active throughout this broad domain of intense deformation but show distinct, uncorrelated

Downloaded from http://pubs.geoscienceworld.org/gsa/geosphere/article-pdf/18/6/1752/5737985/ges02478.1.pdf
by San Jose State Univ King Library Periodicals user

patterns. Cretaceous migration of the axis of arc magmatism at a rate of ~2.6 km/m.y. continued, crossing the actively deforming area ca. 105–85 Ma (Ardill et al., 2018). Neither the location nor kinematics of active deformation followed this eastward sweep of magmatism through time as was previously proposed (Fig. 10; cf. Tobisch et al., 1995; Nadin et al., 2016). Instead, marked shifts in the extent, locus, kinematics, and incremental strain magnitude of mid-Cretaceous deformation occurred ca. 105, 100, 96, and 82 Ma (Figs. 8, 10):

(1) Relative tectonic quiescence until ca. 110–103 Ma suggests that the Sierra Nevada arc experienced little or no deformation during the ca. 130–120 Ma initiation of the Cretaceous arc flare-up. Mid-Cretaceous intra-arc contraction initiated by ca. 105 Ma (Fig. 9). Pluton emplacement occurred over an ~30-km-wide swath in the axial CSN, which only partially overlapped with the western edge of coeval deformation (Fig. 10). The broad domain of ca. 105–100 Ma active contraction was characterized by (1) variable orientations of structural features and, by proxy, variable strain orientations; (2) variable degrees of shear zone development and fabric intensity indicative of heterogeneous strain intensity; (3) variable timing of deformation indicative of protracted contraction over ≥5 m.y.; and (4) downward transfer of surface deposits to the levels of emplacement of hypabyssal intrusions and subsequently upper-crustal plutons (Figs. 8, 9).

(2) Dextral transpressional shear zones initiated within the broad deforming domain by ca. 100–99 Ma or slightly earlier (Figs. 8, 9), signaling the beginning of an ~4–5-m.y.-long, protracted kinematic transition. Localized deformation continued along reverse-sense shear zones following the initiation of dextral transpression. The extent of active deformation remained persistently broad throughout this time. As the kinematic transition progressed, penetrative fabric development occurred over progressively narrower areas centered on active shear zones, indicating localization during progressive deformation (Fig. 10). Magmatic fabrics continued to display highly variable orientations across earliest Late Cretaceous (ca. 99–96 Ma) plutons, indicating that they did not develop within a single-scale uniform flow field (Fig. 9). At the same time, these earliest Late Cretaceous intrusions continued to show no consistent spatiotemporal relationship to the loci of deformation. Maximum shortening directions remained heterogeneous, consistent with partitioned, local flow fields that developed in these transiently incompetent domains (Fig. 9). Downward transfer of surface

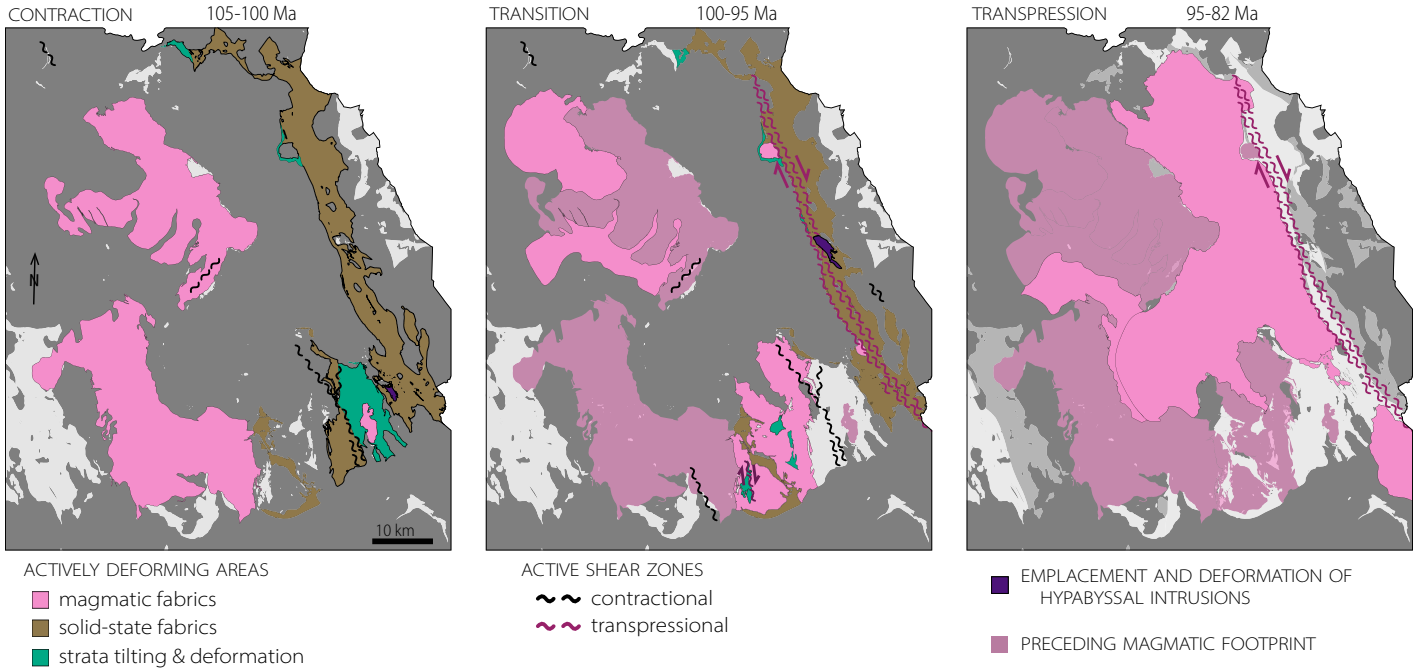

Figure 10. Summary maps of successive intervals of mid-Cretaceous structural development in the central Sierra Nevada, highlighting the distinct patterns of magmatism and deformation during the protracted transition from contraction to dextral transpression. Magmatism occurs both within and away from actively deforming areas at each time interval, with no consistent spatiotemporal coincidence between the two phenomena.

Downloaded from http://pubs.geoscienceworld.org/gsa/geosphere/article-pdf/18/6/1752/5737985/ges02478.1.pdf
by San Jose State Univ King Library Periodicals user

deposits and hypabyssal intrusions to upper-crustal pluton emplacement depths also continued.

(3) Widespread penetrative fabric development in preserved metamorphic strata and activity along reverse-sense shear zones ceased by ca. 97–95 Ma, marking the end of the protracted kinematic transition (Fig. 8). Subsequent ductile deformation was limited to the northern Sierra Crest shear zone, signaling a marked decrease in the extent of active deformation. The ca. 95–84 Ma plutons continued to show a wide range of magmatic fabric orientations and were emplaced across a much wider swath of the axial to eastern CSN than that occupied by the northern Sierra Crest shear zone (Figs. 9, 10).

(4) Ductile deformation continued along the northern Sierra Crest shear zone until a ca. 82–80 Ma transition to a brittle fault system following the cessation of arc magmatism (Jiang and Bentley, 2012; Jiang, 2014; Cao et al., 2015; Cao, 2016). This brittle deformation overprinted earlier ductile fabrics (Hartman et al., 2018). As the arc cooled off, the Sierra Crest shear zone system transitioned into a dextral (± contraction?) brittle fault system (Pachell and Evans, 2002; Compton et al., 2017).

The ca. 100–96 Ma timing of the kinematic transition established herein differs markedly in timing, duration, and character than previous proposals (see also Krueger and Yoshinobu, 2018; cf. Greene and Schweickert, 1995; Tobisch et al., 1995; Tikoff and de Saint Blanquat, 1997; Cao et al., 2015; Nadin et al., 2016). The ca. 96 Ma culmination of this transition saw a significant decrease in the amount of arc-normal shortening. Strain estimates from reverse-sense shear zones are indicative of as much as tens of kilometers of arc-normal shortening accommodated along such structures prior to ca. 96 Ma (Tobisch et al., 1993; Tong, 1994; McNulty, 1995; Cao et al., 2016). Estimates of mid-Cretaceous shortening related to penetrative deformation outside of localized shear zones (prior to ca. 96 Ma) vary from 0% to 30% across an ~50-km-wide zone, corresponding to ~10 km of arc-normal shortening (Tobisch et al., 1977, 2000; Horsman et al., 2008; Cao et al., 2016). In comparison, strain analyses from segments of the northern Sierra Crest shear zone provide estimates of horizontal shortening from ~20% (Mookerjee et al., 2016) to as high as ~75% (Bentley, 2004; Horsman et al., 2008) throughout the ca. 100–80 Ma span of ductile deformation. This corresponds to at most a few kilometers of arc-normal shortening along the ~5-km-wide northern Sierra Crest shear zone, some of which must have occurred before ca. 96 Ma. As the sole locus of significant penetrative deformation after ca. 96 Ma (Fig. 10), the northern Sierra Crest shear zone cannot account for all of the arc-normal shortening that was previously accommodated across the integrated width of active shear zones and penetratively deformed wall rocks ca. 105–96 Ma. These conservative estimates thus require a substantial decrease in the magnitude of intra-arc contraction ca. 96 Ma.

It is important to note that there is no evidence for significant mid-Cretaceous horizontal extension in the CSN aside from the single ambiguous kinematic interpretation of the Courtright-Wishon shear zone. Although Tobisch et al. (1986) postulated that initial Early Cretaceous extensional faulting was followed by mid-Cretaceous contraction, this model was subsequently rejected categorically due to a lack of supporting evidence (Tobisch et al., 2000). We emphasize this point so that future workers will avoid further invoking this untenable model. Some hypabyssal intrusions interpreted as subvertical to vertical sills and dikes may indicate limited, local, and transient dilation parallel to the broader intra-arc shortening direction ca. 102–100 Ma, but only in the uppermost crust. The Minarets caldera and other volcanic deposits were cut and tilted by contractional shear zones and penetratively deformed shortly after deposition, indicating formation during arc-normal shortening at both local and regional scales (Fig. 9; cf. Hughes and Mahood, 2011). Mid-Cretaceous plutons were likewise syn-tectonically emplaced across contractional and transpressional shear zones that continued to accommodate arc-normal shortening during and after emplacement (Fig. 10).

Tectonomagmatic Links

Spatiotemporal patterns of magmatism and deformation reveal indirect tectonomagmatic links between intrusive bodies and shear zones at upper-crustal levels throughout the entire mid-Cretaceous orogenic episode. Magmatism and deformation both took place within a broad, dynamic domain instead of deformation tracking the migrating magmatic and thermal axes of arc activity (cf. Tobisch et al., 1995; Nadin et al., 2016). Magmatism continued its sweep across the broad actively deforming region ca. 105–96 Ma, but active deformation did not decrease in extent nor did its boundaries shift with the axis of arc activity (Fig. 10). Similarly, the location and timing of dextral transpressional shear zones do not correspond to arc migration (cf. Bentley, 2004). Plutons coeval with the ca. 102 Ma initiation of the Bench Canyon shear zone were emplaced tens of kilometers to the west (Fig. 9). The Quartz Mountain shear zone developed well west of any coeval ca. 100 Ma plutons. The northern Sierra Crest shear zone initiated before ca. 98 Ma, when magmatic activity was centered tens of kilometers to the west. By ca. 96 Ma, active ductile deformation within the CSN was limited to the northern Sierra Crest shear zone, with magmatism occurring over a much wider area (Fig. 10). Thus, CSN plutons did not control the location or kinematics of shear zones. This is further supported by mid-Cretaceous hypabyssal intrusions exposed in the Ritter Range pendant that intruded metamorphic wall-rock strata both within and between the northern Sierra Crest shear zone and Bench Canyon shear zone (Fig. 4), with no apparent relationship between these intrusions and deformation.

In turn, CSN shear zones did not control the spatiotemporal patterns of magmatism. Previous arguments for direct tectonomagmatic links, particularly models of pluton emplacement accommodated by dilational features within strike-slip or transpressional shear zones (e.g., Glazner, 1991; Tikoff and Teyssier, 1992), are inconsistent with the synthesis presented herein (see also Yoshinobu et al., 1998). CSN magmatism shows no particular relationship with the timing or location of intra-arc transcurrent motion. First, transpressional and/or strike-slip shear zones do not bound both sides of intrusive bodies

Downloaded from http://pubs.geoscienceworld.org/gsa/geosphere/article-pdf/18/6/1752/5737985/ges02478.1.pdf
by San Jose State Univ King Library Periodicals user

as required by such models (Fig. 9). Specifically, no transpressional shear zones are found along the western boundaries of the Tuolumne and John Muir Intrusive Suites. Second, intra-arc strike-slip or transpressional shear zones are not required for the ascent and emplacement of large magma volumes (e.g., Neves et al., 1996). The voluminous Yosemite Valley and Buena Vista Crest intrusive suites preceded any transcurrent deformation within the CSN. Third, the timing of shear-zone activity does not consistently correspond to the emplacement of particular intrusions, and vice versa. For example, Titus et al. (2005) invoked interactions between the hypothetical northward terminus of the Bench Canyon shear zone and the northern Sierra Crest shear zone to explain emplacement of the ca. 89–87 Ma Johnson Granite Porphyry phase of the Tuolumne Intrusive Suite (Ardill et al., 2020b). Our updated synthesis reveals that any significant Bench Canyon shear zone deformation had ceased prior to the start of Tuolumne construction.

Even where a particular intrusion is coincident with an active shear zone, this cannot be used to argue for direct tectonomagmatic links. Unless a consistent pattern of intrusions overlapping in time and space with specific structural features is established at the appropriate scale of observation, isolated instances of overlap may be a product of coincidental overlap between two phenomena randomly distributed in space and time (e.g., de Bremond d'Ars et al., 1995; Paterson and Schmidt, 1999). These models are incompatible with the mid-Cretaceous tectonomagmatic history of the CSN on the basis of which they were originally formulated, requiring critical reevaluation. Models invoking a close relationship between magmatic weakening and localization of transcurrent motion into arcs, which may or may not include a feedback between magma emplacement and strike-slip motion (e.g., Tommasi et al., 1994; Tobisch and Cruden, 1995; Hutton and Reavy, 1992; de Saint Blanquat et al., 1998; McCaffrey et al., 2000; Cooke et al., 2020), are also incompatible with the lack of consistent spatiotemporal coincidence between magmatism and transpressional shear-zone activity. Similarly, no evidence exists for preferential magma transport along thrust faults (cf. Galland et al., 2003, 2007; Tibaldi, 2005, 2008; Montanari et al., 2010; Ferré et al., 2012).

The synthesis presented herein further demonstrates that voluminous magmas can be emplaced during arc-normal, horizontal contraction without invoking direct tectonomagmatic links. Widespread intra-arc contraction does not seem to suppress magma emplacement or ascent within transcrustal plumbing systems, nor is extension required to explain the emplacement of voluminous plutons (Hutton, 1997; Tibaldi, 2005; Tibaldi et al., 2010; Acocella et al., 2018). Magma ascent is at least partly driven by buoyancy (Spence and Turcotte, 1985; Miller and Paterson, 1999; Vigneresse and Clemens, 2000), a property not directly affected by crustal deformation. Deformation both within and outside of shear zones also cannot significantly disrupt transcrustal magmatic plumbing systems due to the much longer time scales of orogenic strain accumulation relative to the rates of magma transport within even narrow conduits (Pfiffner and Ramsay, 1982; Paterson and Tobisch, 1992; Cañón-Tapia and Walker, 2004; de Saint Blanquat et al., 2011; Sparks and Cashman, 2017). The observed shifts in the isotopic compositions of mid-Cretaceous CSN plutons as the axis of arc magmatism migrated across inherited boundaries between lithospheric domains (Lackey et al., 2008, 2012; Ardill et al., 2018; Ardill, 2020) are a clear example of indirect, arc-scale tectonomagmatic links mediated by lithospheric architecture. The structural and petrologic trends seen across the transition from oceanic to continental basement in the Peninsular Ranges batholith (southern California and Baja California, Mexico) are another such example (e.g., Schmidt et al., 2009; Morton et al., 2014).

Indirect tectonomagmatic links operating at more local scales are also evident in the CSN. Where plutons and hypabyssal intrusions are emplaced into or across mid-Cretaceous shear zones, continued syn- to post-magmatic deformation within these intrusions differs in character from that observed within the surrounding wall rocks. For example, ductile deformation in syn-kinematic intrusions into the Bench Canyon shear zone, including a porphyritic gabbro body and protrusions of the Red Devil Lake and Mount Givens plutons (Fig. 5), occurred at higher temperatures than in the surrounding mylonitic metavolcanic wall rocks (McNulty, 1995). Syn- to post-emplacement solid-state deformation within these intrusions was accommodated by discrete, millimeter- to centimeter-scale, ductile-brittle shear bands that form disorganized networks in outcrop (Fig. 5; McNulty, 1995). These disorganized shear networks contrast with the broad mylonite zones that give way to progressively less intensely developed solid-state foliations where the Bench Canyon shear zone deforms metamorphic wall-rock strata. Where magmatism and deformation overlap, they may influence the local expression of one another even without any direct tectonomagmatic links.

Where mid-Cretaceous CSN plutons experienced post-emplacement deformation, solid-state fabrics are overwhelmingly developed within localized syn- to post-magmatic shear zones (Fig. 9), showing a progression from hypersolidus to subsolidus deformation conditions (e.g., Memeti et al., 2010a; Ardill et al., 2018). The lack of widespread penetrative fabric development in these plutons, though fully crystallized and still warm, indicates that these undeformed intrusions were rheologically stronger than the surrounding wall rocks on the time scales of orogenic strain accumulation (cf. Neves et al., 1996), at least with respect to pure shearing deformation (e.g., Lin et al., 1998; Jiang, 2014). Thus, mid-Cretaceous magmatic bodies in the CSN behaved as stronger phases across multiple scales, even in large plutons, despite millions of years of sustained high temperatures and intermittent melt-present conditions (e.g., Paterson et al., 2011, 2016; Frazer et al., 2014). At a larger scale, both the extent of active intra-arc deformation and amount of strain accommodated within the CSN decreased significantly ca. 96 Ma despite continued high-volume magma additions (Figs. 2, 10). Meanwhile, shortening continued in other across-strike segments of the southwestern U.S. Cordilleran orogen throughout the Late Cretaceous (e.g., Yonkee and Weil, 2015; Thacker et al., 2022). Counterintuitively, the whole orogen–scale partitioning of shortening out of the arc and into across-strike domains (Fig. 11) implies that arc lithosphere became rheologically stronger even as the Cretaceous arc flare-up continued, despite thermomechanical weakening due to increased temperatures and the presence of melts. This apparent increase in competence suggests that

Downloaded from http://pubs.geoscienceworld.org/gsa/geosphere/article-pdf/18/6/1752/5737985/ges02478.1.pdf
by San Jose State Univ King Library Periodicals user

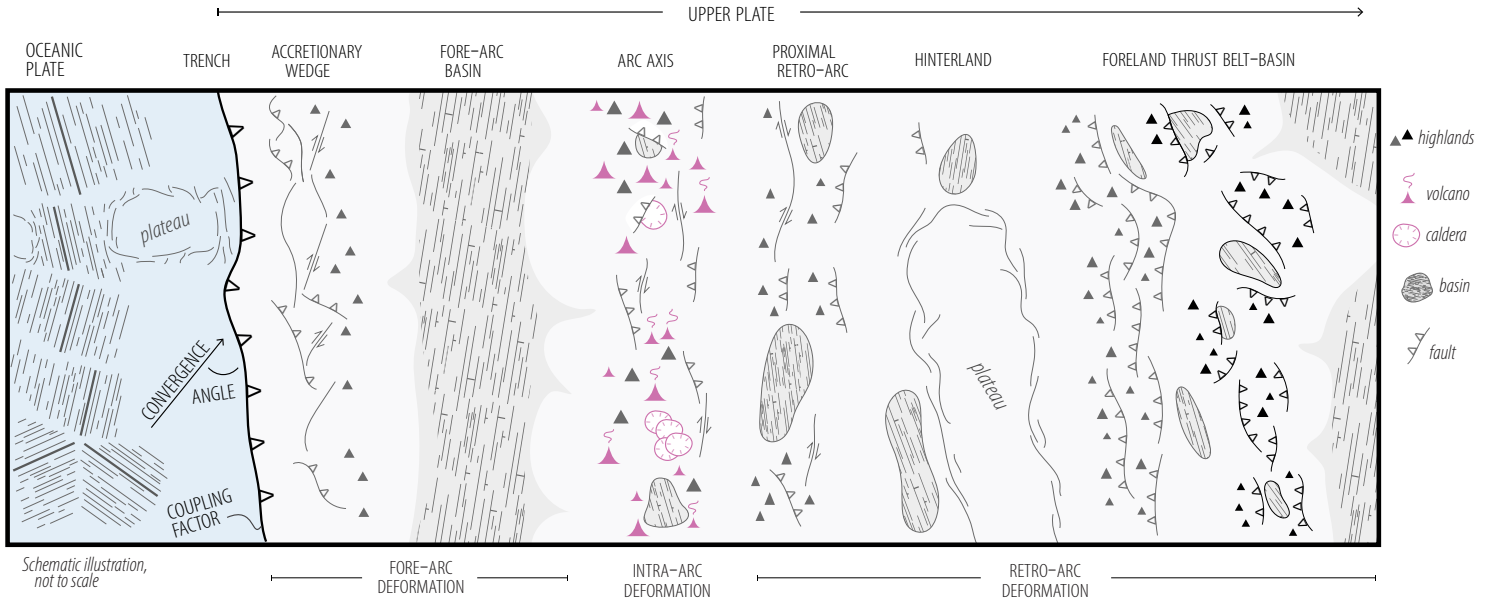

Figure 11. Schematic cartoon of structural development across an entire convergent margin orogenic system, loosely based on the Cretaceous–Paleogene western North American Cordillera. Changes in deformation observed in any one across-strike region may be related to shifting boundary conditions and/or orogen-scale partitioning.

some processes attendant to arc and orogenic activity discussed further below strengthen the lithosphere.

Controls of Shifting Deformation Partitioning

The mid-Cretaceous CSN orogenic episode is characterized by heterogeneous, non-steady deformation at all scales of observation:

(1) The consistently high range in orientations of tectonically significant magmatic foliations during each phase of the mid-Cretaceous orogenic episode indicates that these fabrics record strain orientations within partitioned local flow fields (cf. Cao et al., 2015) consistent with micromechanics for the deformation of heterogeneous materials (Jiang, 2014).

(2) The variable orientations of composite foliations in pre-Cretaceous wall-rock strata in the CSN (Fig. 9) at least partially reflect the influence of pre-existing rheological anisotropy on the orientation and intensity of the mid-Cretaceous component of these composite fabrics.

(3) Variable orientations of bedding in tilted Cretaceous strata as well as variable orientations and kinematics of localized shear zones are indicative of heterogeneous maximum shortening directions even without the influence of pre-existing anisotropy.

Factors other than compositionally controlled competency contrasts are required to explain such partitioning (Fig. 12; Cao et al., 2016).

The structural impacts of arc magmatism, both rheological and dynamic, likely played a key role in this deformation partitioning, even without direct control on the spatiotemporal patterns of deformation. Arc activity modifies deformation fields both locally, through mechanical, thermal, and chemical stresses related to a single intrusion (Hutton, 1997; Karlstrom et al., 2009; Ruch et al., 2016), and regionally, through crustal column-scale downward transfer of host rocks to isostatically compensate for voluminous magmatic addition and/or contraction accompanied by only limited exhumation (Paterson and Farris, 2008; Cao et al., 2016). The gravitational effect of volcanic-edifice construction at the surface may also locally dominate stress fields in the uppermost crust (Nakamura, 1977). Preserved instances of deformation related to the local-scale impacts of mid-Cretaceous pluton construction are limited (e.g., Yoshinobu et al., 2009; Pignotta et al., 2010; Memeti et al., 2022). Mid-Cretaceous downward transfer of host rocks relative to the arc surface was likely accommodated by the combined effects of (1) burial by overlying erupted volcanic products and within the footwall of reverse-sense shear zones and (2) downward "flow" of host rocks in response to crustal thickening accompanied by limited exhumation (Cao and Paterson, 2016). Yet no localized structures accommodating downward transfer have been observed outside of

Downloaded from http://pubs.geoscienceworld.org/gsa/geosphere/article-pdf/18/6/1752/5737985/ges02478.1.pdf
by San Jose State Univ King Library Periodicals user

the narrow aureoles of mid-Cretaceous plutons (Cao et al., 2016). Downward "flow" apparently operated at crustal-column scales such that entire crustal levels moved downward relative to the arc surface.

Arc activity also influences rheology, including some processes that may strengthen the lithosphere. At the local scale, flare-up magmatism introduces progressively greater proportions of coarse-grained, feldspar-rich plutonic rocks that represent more competent rheological domains relative to the surrounding upper-crustal host rocks. Plutons apparently represent competent inclusions on the time scales of orogenic strain accumulation, even in the case where several long-lived magmatic suites are constructed across a wide portion of the arc (Paterson and Tobisch, 1992; Petford et al., 2000). Increased contrasts in effective viscosity and stress-strain perturbations developed around rheological heterogeneities further contribute to deformation partitioning (Fig. 12). Elongate plutons exhibiting shape-preferred orientation can create anisotropy external to individual intrusions (Perry-Houts and Karlstrom, 2019).

Voluminous flare-up magmatism may affect the bulk rheology of arc lithosphere at regional scales as well. Plutons might also disrupt major throughgoing shear zones that control the "bulk" yield strength of the entire crust (Platt and Behr, 2011). Magmatism and contraction together modify lithospheric architecture via thickening, formation of a dense root, and addition of buoyant plutonic material to the crust accompanied by the formation of mafic magmatic residues in the lower crust. The formation of a thick, dense arc root during flare-ups or the addition of competent mafic residues to lower-arc crust may strengthen the entire lithospheric column by modifying rheology at a single crustal level. At even greater scales, these effects may make arc

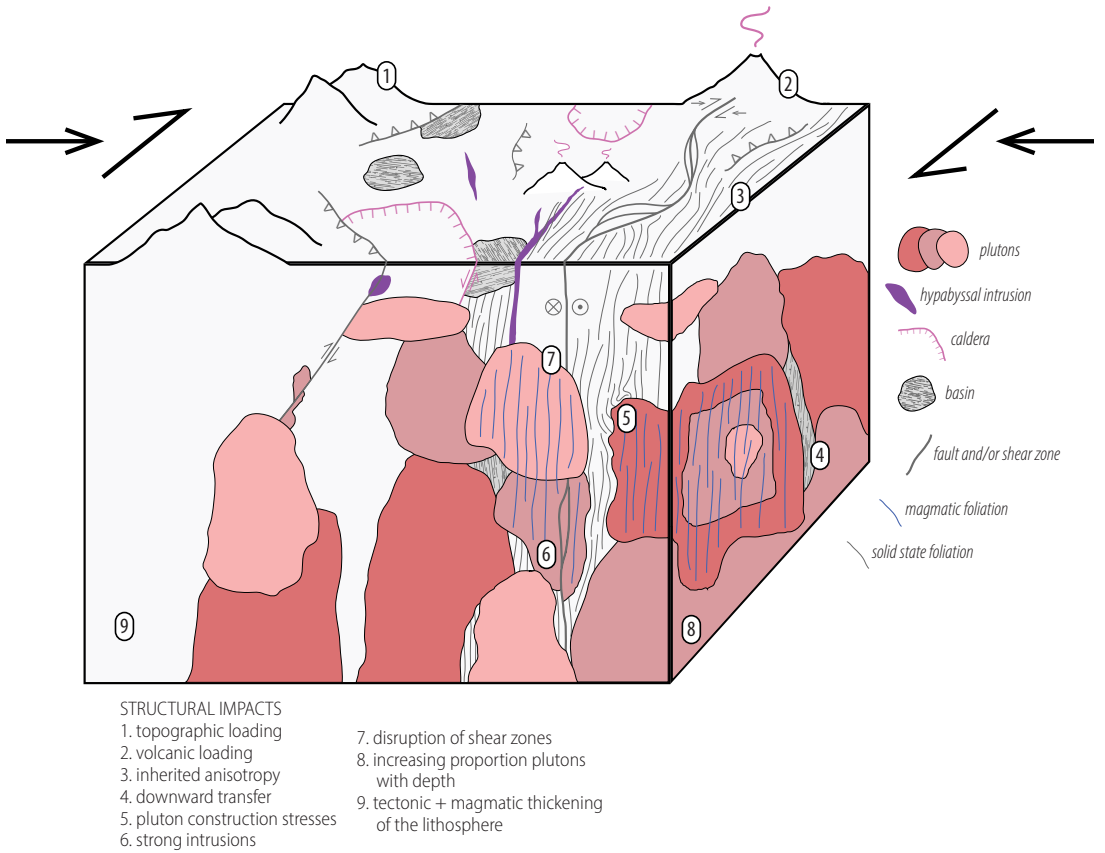

Figure 12. Schematic cartoon of structural impacts of arc activity and magmatic-tectonic interactions.

Downloaded from http://pubs.geoscienceworld.org/gsa/geosphere/article-pdf/18/6/1752/5737985/ges02478.1.pdf
by San Jose State Univ King Library Periodicals user

lithosphere more competent than surrounding regions across strike of the margin. At the same time, changes in lithospheric thickness and density may impact mantle-wedge and subduction dynamics, in effect modifying the boundary conditions that drive arc and orogenic activity in the first place (Chin et al., 2012; Karlstrom et al., 2014; Holt et al., 2015).

In this way, heterogeneous deformation, driven by imposed tectonic boundary conditions, was influenced by the rheological impacts of magmatism but also, in turn, further modified the structural response to arc activity. This heterogeneous and shifting structural development influenced by far-field, regional, and local factors indicates that mid-Cretaceous deformation in the CSN did not directly reflect far-field plate-boundary conditions as depicted in a single-scaled homogeneous model (cf. Nadin et al., 2016). Mid-Cretaceous deformation almost certainly shifted through time in response to changing plate dynamics (Tobisch et al., 1995) and also evolving lithospheric rheology (Lister and Williams, 1983). The observed mid-Cretaceous kinematic transition to dextral transpression may have been driven by increasingly oblique plate convergence at the subduction zone. Alternatively, the ca. 100 Ma addition of transcurrent components to CSN deformation may have been caused by progressive partitioning of strike-slip motion into the arc under far-field convergence with a consistent obliquity (Fig. 11). Such shifts in partitioned deformation may be due to the progressive evolution of shear-zone systems (e.g., Cooke et al., 2020) and/or shifts in rheology due to the lithospheric evolution that attends arc and orogenic activity (Fig. 12).

CONCLUSIONS

Deformation partitioning is ubiquitous across all scales of observation and is influenced by the structural impacts of arc activity that operate across scale, time, and space (Figs. 11, 12). Arc activity contributes to partitioned deformation fields in unexpected ways on both local and regional scales. Plutons, for example, appear to behave as competent inclusions on the time scales of orogenic strain accumulation whereas high magmatic addition rates drive extensive reworking of arc lithosphere. While the broadly NNW-trending structural and magmatic grain of the Sierra Nevada arc reflects the boundary conditions imposed by plate tectonics, the arc did not behave as a uniformly deforming block. Small-scale structural observations of intrusions, host rocks, shear zones, faults, folds, and fabrics are more readily understood as products of local flow fields rather than directly reflecting far-field boundary conditions.

Even with this well constrained record of central Sierra Nevada deformation (Fig. 9), it is not straightforward to interpret paleo–plate dynamics or the intra-arc strain field. A multi-order perspective that spans small-scale structures to the whole orogen, from the accretionary wedge to the foreland, is needed to decipher the links between plate-scale geodynamics, lithospheric evolution, and tectonism at convergent margins. Convergence at the subduction zone, modified by convergence angle and the degree of downgoing slab–overriding plate coupling, must be accommodated by the sum of deformation partitioned into the fore-, intra-, and retro-arc regions (Fig. 11). Both subduction dynamics and orogen-scale partitioning can vary with time and are not easily disentangled in the rock record of upper-plate deformation. The thermal, mechanical, compositional, and petrological impacts of arc activity at different crustal levels must all be considered to determine the evolution of lithospheric rheology. The issues raised herein are likely to apply outside of the Sierra Nevada as well. Postulated links between tectonism, magmatism, and plate dynamics proposed in other arc and orogenic systems likely need to be revisited and either conclusively demonstrated or rejected, requiring a broad shift in the conceptual framework that underlies new investigations.

ACKNOWLEDGMENTS

We thank Wenrong Cao, Vali Memeti, Katie Ardill, Sean Hartman, and Cullen Scheland for insightful discussions; James King, Simon Crosbie, Yu Chuan Shan, Richard Brown, Abigail Wesley, Henry Hoult, Alexander Arita, and Solishia Andico for their help in the field; Frontier Pack Train, Minarets Pack Station, and Red's Meadow Pack Station personnel for their invaluable services; and Valerio Acocella, Andrea Hampel, Aaron Yoshinobu, and an anonymous reviewer for their review and consideration of this manuscript. We also gratefully acknowledge helpful comments from John Platt, Alexander Lusk, and Jacob Thacker on earlier versions of this manuscript. This work was supported by a Canadian Natural Sciences and Engineering Research Council discovery grant to Dazhi Jiang; U.S. National Science Foundation grants EAR-1624847, EAR-1524798, EAR-1019636, and EAR-0948680 to Scott R. Paterson and EAR-0074099 and EAR-9614758 to Robert B. Miller; U.S. Geological Survey EDMAP grants 08HQAG0057, G12AC20178, G13AC00120, G15AC00134, and G16AC00160 to Scott R. Paterson and G13AC00118 to Robert B. Miller; and a Geological Society of America Graduate Student Research Grant awarded to Snir Attia.

REFERENCES CITED

Acocella, V., 2014, Structural control on magmatism along divergent and convergent plate boundaries: Overview, model, problems: Earth-Science Reviews, v. 136, p. 226–288, https://doi.org/10.1016/j.earscirev.2014.05.006.

Acocella, V., and Funiciello, F., 2010, Kinematic setting and structural control of arc volcanism: Earth and Planetary Science Letters, v. 289, p. 43–53, https://doi.org/10.1016/j.epsl.2009.10.027.

Acocella, V., Bellier, O., Sandri, L., Sebrier, M., and Pramumijoyo, S., 2018, Weak tectono-magmatic relationships along an obliquely convergent plate boundary: Sumatra, Indonesia: Frontiers of Earth Science, v. 6, no. 3, https://doi.org/10.3389/feart.2018.00003.

Allmendinger, R.W., Cardozo, N., and Fisher, D.M., 2012, Structural Geology Algorithms: Vectors and Tensors: Cambridge, UK, Cambridge University Press, 289 p.

Ardill, K.E., 2020, Spatial and temporal evolution of magmatic systems in continental arcs: A case study of dynamic arc behaviors in the Mesozoic Sierra Nevada, California [Ph.D. thesis]: Los Angeles, University of Southern California, 333 p.

Ardill, K.E., Paterson, S.R., and Memeti, V., 2018, Spatiotemporal magmatic focusing in upper-mid crustal plutons of the Sierra Nevada arc: Earth and Planetary Science Letters, v. 498, p. 88–100, https://doi.org/10.1016/j.epsl.2018.06.023.

Ardill, K., Memeti, V., and Paterson, S., 2020a, Reconstructing the physical and chemical development of a pluton-porphyry complex in a tectonically reorganized arc crustal section, Tioga Pass, Sierra Nevada: Lithosphere, v. 2020, 8872875, https://doi.org/10.2113/2020/8872875.

Ardill, K.E., Paterson, S.R., Stanback, J., Alasino, P.H., King, J.J., and Crosbie, S.E., 2020b, Schlieren-bound magmatic structures record crystal flow-sorting in dynamic upper-crustal magma-mush chambers: Frontiers of Earth Science, v. 8, 190, https://doi.org/10.3389/feart.2020.00190.

Armstrong, R.L., and Ward, P.L., 1993, Late Triassic to earliest Eocene magmatism in the North American Cordillera: Implications for the Western Interior Basin, *in* Caldwell, W.G.E., and Kauffman, E.G., eds., Evolution of the Western Interior Basin: Geological Association of Canada Special Paper 39, p. 49–72.

Downloaded from http://pubs.geoscienceworld.org/gsa/geosphere/article-pdf/18/6/1752/5737985/ges02478.1.pdf
by San Jose State Univ King Library Periodicals user

Asmerom, Y., Patchett, P.J., and Damon, P.E., 1991, Crust-mantle interaction in continental arcs: Inferences from the Mesozoic arc in the southwestern United States: Contributions to Mineralogy and Petrology, v. 107, p. 124–134, https://doi.org/10.1007/BF00311190.

Attia, S., Paterson, S.R., Cao, W.R., Chapman, A.D., Saleeby, J., Dunne, G.C., Stevens, C.H., and Memeti, V., 2018, Late Paleozoic tectonic assembly of the Sierra Nevada prebatholithic framework and western Laurentian provenance links based on synthesized detrital zircon geochronology, *in* Ingersoll, R.V., Lawton, T.F., and Graham, S.A., eds., Tectonics, Sedimentary Basins, and Provenance: A Celebration of the Career of William R. Dickinson: Geological Society of America Special Paper 540, p. 267–295, https://doi.org/10.1130/2018.2540(12).

Attia, S., Cottle, J.M., and Paterson, S.R., 2020, The erupted zircon record of continental crust formation during mantle driven arc flare-ups: Geology, v. 48, p. 446–451, https://doi.org/10.1130/G46991.1.

Attia, S., Paterson, S.R., Saleeby, J., and Cao, W.R., 2021, Detrital zircon provenance and depositional links of Mesozoic Sierra Nevada intra-arc strata: Geosphere, v. 17, p. 1422–1453, https://doi.org/10.1130/GES02296.1.

Barth, A.P., Walker, J.D., Wooden, J.L., Riggs, N.R., and Schweickert, R.A., 2011, Birth of the Sierra Nevada magmatic arc: Early Mesozoic plutonism and volcanism in the east-central Sierra Nevada of California: Geosphere, v. 7, p. 877–897, https://doi.org/10.1130/GES00661.1.

Barth, A.P., Wooden, J.L., Riggs, N.R., Walker, J.D., Tani, K., Penniston-Dorland, S.C., Jacobson, C.E., Laughlin, J.A., and Hiramatsu, R., 2018, Marine volcaniclastic record of early arc evolution in the eastern Ritter Range pendant, central Sierra Nevada, California: Geochemistry Geophysics Geosystems, v. 19, p. 2543–2559, https://doi.org/10.1029/2018GC007456.

Bartley, J.M., Glazner, A.F., and Coleman, D.S., 2018, Dike intrusion and deformation during growth of the Half Dome pluton, Yosemite National Park, California: Geosphere, v. 14, p. 1283–1297, https://doi.org/10.1130/GES01458.1.

Bateman, P.C., 1992, Plutonism in the central part of the Sierra Nevada batholith, California: U.S. Geological Survey Professional Paper 1483, 186 p., https://doi.org/10.3133/pp1483.

Bateman, P.C., Kistler, R.W., Peck, D.L., and Busacca, A., 1983, Geologic map of the Tuolumne Meadows quadrangle, Yosemite National Park, California: U.S. Geological Survey Geologic Quadrangle Map GQ-1570, 1 sheet, scale 1:62,500, https://doi.org/10.3133/gq1570.

Bateman, P.C., Kistler, R.W., and DeGraff, J.V., 1984, Courtright intrusive zone: Sierra National Forest, Fresno County, California: California Geology, v. 37, p. 91–98.

Benn, K., Paterson, S.R., Lund, S.P., Pignotta, G.S., and Kruse, S., 2001, Magmatic fabrics in batholiths as markers of regional strains and plate kinematics: Example of the Cretaceous Mt. Stuart batholith: Physics and Chemistry of the Earth, Part A: Solid Earth and Geodesy, v. 26, p. 343–354, https://doi.org/10.1016/S1464-1895(01)00064-3.

Bentley, C., 2004, Rock fabric analysis of the Sierra Crest shear zone system, California: Implications for crustal-scale transpressional shear zones [M.S. thesis]: College Park, University of Maryland, 172 p.

Berger, A.R., and Pitcher, W.S., 1970, Structures in granitic rocks: A commentary and critique on granite tectonics: Proceedings of the Geologists' Association of London, v. 81, p. 441–461, https://doi.org/10.1016/S0016-7878(70)80006-2.

Burchfiel, B.C., and Davis, G.A., 1972, Structural framework and evolution of the southern part of the Cordilleran orogen, western United States: American Journal of Science, v. 272, p. 97–118, https://doi.org/10.2475/ajs.272.2.97.

Burgess, S.D., and Miller, J.S., 2008, Construction, solidification, and internal differentiation of a large felsic arc pluton: Cathedral Peak granodiorite, Sierra Nevada Batholith, *in* Annen, C., and Zellmer, G.F., eds., Dynamics of Crustal Magma Transfer, Storage and Differentiation: Geological Society of London Special Publication 304, p. 203–233, https://doi.org/10.1144/SP304.11.

Burgess, S.D., Bowring, S.A., Petsche, J., Miller, R.B., and Miller, J.S., 2009, High precision U-Pb CA-TIMS geochronology for the Sentinel and Yosemite Creek Granodiorites, Sierra Nevada batholith, CA: A history of punctuated intrusion and protracted crystallization: Abstract V42A-05 presented at American Geophysical Union Fall Meeting 2009, San Francisco, California, 14–18 December.

Callahan, C.N., and Markley, M.J., 2003, A record of crustal-scale stress: Igneous foliation and lineation in the Mount Waldo Pluton, Waldo County, Maine: Journal of Structural Geology, v. 25, p. 541–555, https://doi.org/10.1016/S0191-8141(02)00052-4.

Cañón-Tapia, E., and Walker, G.P.L., 2004, Global aspects of volcanism: The perspective of "plate tectonics" and "volcanic systems": Earth-Science Reviews, v. 66, p. 163–182, https://doi.org/10.1016/j.earscirev.2003.11.001.

Cao, W.R., 2016, Links, tempos, and mass balances of cyclic deformation and magmatism in arcs: A case study on the Mesozoic Sierra Nevada arc integrating geological mapping, geochronology, geobarometry, strain analyses and numerical simulations [Ph.D. thesis]: Los Angeles, University of Southern California, 410 p., https://doi.org/10.25549/uscthesis-c3-615210.

Cao, W.R., and Paterson, S., 2016, A mass balance and isostasy model: Exploring the interplay between magmatism, deformation and surface erosion in continental arcs using central Sierra Nevada as a case study: Geochemistry Geophysics Geosystems, v. 17, p. 2194–2212, https://doi.org/10.1002/2015GC006229.

Cao, W., Paterson, S., Memeti, V., Mundil, R., Anderson, J.L., and Schmidt, K., 2015, Tracking paleodeformation fields in the Mesozoic central Sierra Nevada arc: Implications for intra-arc cyclic deformation and arc tempos: Lithosphere, v. 7, p. 296–320, https://doi.org/10.1130/L389.1.

Cao, W.R., Paterson, S.R., Saleeby, J., and Zalunardo, S., 2016, Bulk arc strain, crustal thickening, magma emplacement, and mass balances in the Mesozoic Sierra Nevada arc: Journal of Structural Geology, v. 84, p. 14–30, https://doi.org/10.1016/j.jsg.2015.11.002.

Cardozo, N., and Allmendinger, R.W., 2013, Spherical projections with OSXStereonet: Computers & Geosciences, v. 51, p. 193–205, https://doi.org/10.1016/j.cageo.2012.07.021.

Cecil, M.R., Rotberg, G.L., Ducea, M.N., Saleeby, J.B., and Gehrels, G.E., 2012, Magmatic growth and batholithic root development in the northern Sierra Nevada, California: Geosphere, v. 8, p. 592–606, https://doi.org/10.1130/GES00729.1.

Cecil, M.R., Rusmore, M.E., Gehrels, G.E., Woodsworth, G.J., Stowell, H.H., Yokelson, I.N., Chisom, C., Trautman, E., and Homan, E., 2018, Along-strike variation in the magmatic tempo of the Coast Mountains batholith, British Columbia, and implications for processes controlling episodicity in arcs: Geochemistry Geophysics Geosystems, v. 19, p. 4274–4289, https://doi.org/10.1029/2018GC007874.

Cecil, M.R., Ferrer, M.A., Riggs, N.R., Marsaglia, K., Kylander-Clark, A., Ducea, M.N., and Stone, P., 2019, Early arc development recorded in Permian–Triassic plutons of the northern Mojave Desert region, California, USA: Geological Society of America Bulletin, v. 131, p. 749–765, https://doi.org/10.1130/B31963.1.

Chambers, M., Memeti, V., Eddy, M.P., and Schoene, B., 2020, Half a million years of magmatic history recorded in a K-feldspar megacryst of the Tuolumne Intrusive Complex, California, USA: Geology, v. 48, p. 400–404, https://doi.org/10.1130/G46873.1.

Chapman, J.B., and Ducea, M.N., 2019, The role of arc migration in Cordilleran orogenic cyclicity: Geology, v. 47, p. 627–631, https://doi.org/10.1130/G46117.1.

Chapman, J.B., Shields, J.E., Ducea, M.N., Paterson, S.R., Attia, S., and Ardill, K.E., 2021, The causes of continental arc flare ups and drivers of episodic magmatic activity in Cordilleran orogenic systems: Lithos, v. 398–399, 106307, https://doi.org/10.1016/j.lithos.2021.106307.

Chen, J.H., and Moore, J.G., 1982, Uranium-lead isotopic ages from the Sierra Nevada Batholith, California: Journal of Geophysical Research, v. 87, p. 4761–4784, https://doi.org/10.1029/JB087iB06p04761.

Chin, E.J., Lee, C.-T.A., Luffi, P., and Tice, M., 2012, Deep lithospheric thickening and refertilization beneath continental arcs: Case study of the *P*, *T* and compositional evolution of peridotite xenoliths from the Sierra Nevada, California: Journal of Petrology, v. 53, p. 477–511, https://doi.org/10.1093/petrology/egr069.

Coleman, D.S., and Glazner, A.F., 1997, The Sierra Crest magmatic event: Rapid formation of juvenile crust during the Late Cretaceous in California: International Geology Review, v. 39, p. 768–787, https://doi.org/10.1080/00206819709465302.

Coleman, D.S., Gray, W., and Glazner, A.F., 2004, Rethinking the emplacement and evolution of zoned plutons: Geochronologic evidence for incremental assembly of the Tuolumne Intrusive Suite, California: Geology, v. 32, p. 433–436, https://doi.org/10.1130/G20220.1.

Compton, K.E., Kirkpatrick, J.D., and Holk, G.J., 2017, Cyclical shear fracture and viscous flow during transitional ductile-brittle deformation in the Saddlebag Lake Shear Zone, California: Tectonophysics, v. 708, p. 1–14, https://doi.org/10.1016/j.tecto.2017.04.006.

Cooke, M.L., Toeneboehn, K., and Hatch, J.L., 2020, Onset of slip partitioning under oblique convergence within scaled physical experiments: Geosphere, v. 16, p. 875–889, https://doi.org/10.1130/GES02179.1.

Cruden, A.R., 1990, Flow and fabric development during the diapiric rise of magma: The Journal of Geology, v. 98, p. 681–698, https://doi.org/10.1086/629433.

Davis, J.W., Coleman, D.S., Gracely, J.T., Gaschnig, R., and Stearns, M., 2012, Magma accumulation rates and thermal histories of plutons of the Sierra Nevada batholith, CA: Contributions to Mineralogy and Petrology, v. 163, p. 449–465, https://doi.org/10.1007/s00410-011-0683-7.

Downloaded from http://pubs.geoscienceworld.org/gsa/geosphere/article-pdf/18/6/1752/5737985/ges02478.1.pdf
by San Jose State Univ King Library Periodicals user

de Bremond d'Ars, J., Jaupart, C., and Sparks, R.S.J., 1995, Distribution of volcanoes in active margins: Journal of Geophysical Research, v. 100, p. 20,421–20,432, https://doi.org/10.1029/95JB02153.

DeCelles, P.G., 2004, Late Jurassic to Eocene evolution of the Cordilleran thrust belt and foreland basin system, western U.S.A.: American Journal of Science, v. 304, p. 105–168, https://doi.org/10.2475/ajs.304.2.105.

DeCelles, P.G., Ducea, M.N., Kapp, P., and Zandt, G., 2009, Cyclicity in Cordilleran orogenic systems: Nature Geoscience, v. 2, p. 251–257, https://doi.org/10.1038/ngeo469.

de Saint Blanquat, M., Tikoff, B., Teyssier, C., and Vigneresse, J.L., 1998, Transpressional kinematics and magmatic arcs, *in* Holdsworth, R.E., Strachan, R.A., and Dewey, J.F., eds., Continental Transpressional and Transtensional Tectonics: Geological Society of London Special Publication 135, p. 327–340, https://doi.org/10.1144/GSL.SP.1998.135.01.21.

de Saint Blanquat, M., Horsman, E., Habert, G., Morgan, S., Vanderharge, O., Law, R., and Tikoff, B., 2011, Multiscale magmatic cyclicity, duration of pluton construction, and the paradoxical relationship between tectonism and plutonism in continental arcs: Tectonophysics, v. 500, p. 20–33, https://doi.org/10.1016/j.tecto.2009.12.009.

Dodge, F.C.W., and Calk, L.C., 1986, Lake Eleanor quadrangle, central Sierra Nevada, California: Analytic data: U.S. Geological Survey Bulletin 1565, 20 p., https://doi.org/10.3133/b1585.

Ducea, M., 2001, The California arc: Thick granitic batholiths, eclogitic residues, lithospheric-scale thrusting, and magmatic flare-ups: GSA Today, v. 11, p. 4–10, https://doi.org/10.1130/1052-5173(2001)011<0004:TCATGB>2.0.CO;2.

Ducea, M.N., and Barton, M.D., 2007, Igniting flare-up events in Cordilleran arcs: Geology, v. 35, p. 1047–1050, https://doi.org/10.1130/G23898A.1.

Engebretson, D.C., Cox, A., and Gordon, R.G., 1985, Relative Motions between Oceanic and Continental Plates in the Pacific Basin: Geological Society of America Special Paper 206, 59 p., https://doi.org/10.1130/SPE206.

Ernst, W.G., Saleeby, J.B., and Snow, C.A., 2009, Guadalupe pluton–Mariposa Formation age relationships in the southern Sierran Foothills: Onset of Mesozoic subduction in northern California?: Journal of Geophysical Research, v. 114, B11204, https://doi.org/10.1029/2009JB006607.

Ferré, E., Gleizes, G., Bouchez, J.L., and Nnabo, P.N., 1995, Internal fabric and strike-slip emplacement of the Pan-African granite of Solli Hills, northern Nigeria: Tectonics, v. 14, p. 1205–1219, https://doi.org/10.1029/95TC01445.

Ferré, E.C., Galland, O., Montanari, D., and Kalakay, T.J., 2012, Granite magma migration and emplacement along thrusts: International Journal of Earth Sciences, v. 101, p. 1673–1688, https://doi.org/10.1007/s00531-012-0747-6.

Fiske, R.S., and Tobisch, O.T., 1978, Paleogeographic significance of volcanic rocks of the Ritter Range pendant, central Sierra Nevada, *in* Howell, D.G., and McDougall, K.A., eds., Mesozoic Paleogeography of the Western United States: Pacific Coast Paleogeography Symposium 2: Los Angeles, Society of Economic Paleontologists and Mineralogists, Pacific Section, p. 209–222.

Fiske, R.S., and Tobisch, O.T., 1994, Middle Cretaceous ash-flow tuff and caldera-collapse deposit in the Minarets Caldera, east-central Sierra Nevada, California: Geological Society of America Bulletin, v. 106, p. 582–593, https://doi.org/10.1130/0016-7606(1994)106<0582:MCAFTA>2.3.CO;2.

Frazer, R.E., Coleman, D.S., and Mills, R.D., 2014, Zircon U-Pb geochronology of the Mount Givens Granodiorite: Implications for the genesis of large volumes of eruptible magma: Journal of Geophysical Research: Solid Earth, v. 119, p. 2907–2924, https://doi.org/10.1002/2013JB010716.

Frost, T.P., 1987, Sample localities, radiometric ages, descriptions, and major- and trace-element abundances of Late Jurassic mafic plutonic rocks, eastern Sierra Nevada, California: U.S. Geological Survey Open-File Report 87-484, 33 p., https://doi.org/10.3133/ofr87484.

Frost, T.P., and Mattinson, J.M., 1988, Late Cretaceous U-Pb age of a mafic intrusion from the eastern Sierra Nevada, California: Isochron/West, v. 51, p. 15–18.

Galland, O., De Bremond d'Ars, J., Cobbold, P.R., and Hallot, E., 2003, Physical models of magmatic intrusion during thrusting: Terra Nova, v. 15, p. 405–409, https://doi.org/10.1046/j.1365-3121.2003.00512.x.

Galland, O., Cobbold, P.R., de Bremond d'Ars, J., and Hallot, E., 2007, Rise and emplacement of magma during horizontal shortening of the brittle crust: Insights from experimental modeling: Journal of Geophysical Research, v. 112, B06402, https://doi.org/10.1029/2006JB004604.

Gehrels, G., Valencia, V., and Pullen, A., 2006, Detrital zircon geochronology by laser-ablation multicollector ICPMS at the Arizona LaserChron Center: The Paleontological Society Papers, v. 12, p. 67–76, https://doi.org/10.1017/S1089332600001352.

Gehrels, G.E., Valencia, V.A., and Ruiz, J., 2008, Enhanced precision, accuracy, efficiency, and spatial resolution of U-Pb ages by laser ablation–multicollector–inductively coupled plasma–mass spectrometry: Geochemistry Geophysics Geosystems, v. 9, Q03017, https://doi.org/10.1029/2007GC001805.

Gelman, S.E., Gutiérrez, F.J., and Bachmann, O., 2013, On the longevity of large upper crustal silicic magma reservoirs: Geology, v. 41, p. 759–762, https://doi.org/10.1130/G34241.1.

Glazner, A.F., 1991, Plutonism, oblique subduction, and continental growth: An example from the Mesozoic of California: Geology, v. 19, p. 784–786, https://doi.org/10.1130/0091-7613(1991)019<0784:POSACG>2.3.CO;2.

Grasse, S.W., Gehrels, G.E., Lahren, M.M., Schweickert, R.A., and Barth, A.P., 2001, U-Pb geochronology of detrital zircons from the Snow Lake pendant, central Sierra Nevada—Implications for Late Jurassic–Early Cretaceous dextral strike-slip faulting: Geology, v. 29, p. 307–310, https://doi.org/10.1130/0091-7613(2001)029<0307:UPGODZ>2.0.CO;2.

Greene, D.C., and Schweickert, R.A., 1995, The Gem Lake shear zone: Cretaceous dextral transpression in the Northern Ritter Range pendant, eastern Sierra Nevada, California: Tectonics, v. 14, p. 945–961, https://doi.org/10.1029/95TC01509.

Hamilton, W., 1969, Mesozoic California and the underflow of Pacific mantle: Geological Society of America Bulletin, v. 80, p. 2409–2430, https://doi.org/10.1130/0016-7606(1969)80[2409:MCATUO]2.0.CO;2.

Hanson, R.B., Sorensen, S.S., Barton, M.D., and Fiske, R.S., 1993, Long-term evolution of fluid-rock interactions in magmatic arcs: Evidence from the Ritter Range pendant, Sierra Nevada, California, and numerical modeling: Journal of Petrology, v. 34, p. 23–62, https://doi.org/10.1093/petrology/34.1.23.

Hartman, S.M., Paterson, S.R., Holk, G.J., and Kirkpatrick, J.D., 2018, Structural and hydrothermal evolution of a strike-slip shear zone during a ductile-brittle transition, Sierra Nevada, CA: Journal of Structural Geology, v. 113, p. 134–154, https://doi.org/10.1016/j.jsg.2018.05.010.

Hildreth, W., and Moorbath, S., 1988, Crustal contributions to arc magmatism in the Andes of Central Chile: Contributions to Mineralogy and Petrology, v. 98, p. 455–489, https://doi.org/10.1007/BF00372365.

Hildreth, W., Fierstein, J., and Ryan-Davis, J., 2021, No ring fracture in Mono Basin, California: Geological Society of America Bulletin, v. 133, p. 2210–2225, https://doi.org/10.1130/B35747.1.

Holt, A.F., Buffett, B.A., and Becker, T.W., 2015, Overriding plate thickness control on subducting plate curvature: Geophysical Research Letters, v. 42, p. 3802–3810, https://doi.org/10.1002/2015GL063834.

Horsman, E., Tikoff, B., and Czeck, D., 2008, Rheological implications of heterogeneous deformation at multiple scales in the Late Cretaceous Sierra Nevada, California: Geological Society of America Bulletin, v. 120, p. 238–255, https://doi.org/10.1130/B26161.1.

Huber, N.K., and Rinehart, C.D., 1965, Geologic map of the Devils Postpile quadrangle, Sierra Nevada, California: U.S. Geological Survey Geologic Quadrangle Map GQ-437, 1 sheet, scale 1:62,500, https://doi.org/10.3133/gq437.

Hughes, G.R., and Mahood, G.A., 2011, Silicic calderas in arc settings: Characteristics, distribution, and tectonic controls: Geological Society of America Bulletin, v. 123, p. 1577–1595, https://doi.org/10.1130/B30232.1.

Hutton, D.H.W., 1997, Syntectonic granites and the principle of effective stress: A general solution to the space problem?, *in* Bouchez, J.L., Hutton, D.H.W., and Stephens, W.E., eds., Granite: From Segregation of Melt to Emplacement Fabrics: Amsterdam, Kluwer Academic Publishers, p. 189–197, https://doi.org/10.1007/978-94-017-1717-5_12.

Hutton, D.H.W., and Reavy, R.J., 1992, Strike-slip tectonics and granite petrogenesis: Tectonics, v. 11, p. 960–967, https://doi.org/10.1029/92TC00336.

Jennings, C.W., with modifications by Gutierrez, C., Bryant, W., Saucedo, G., and Wills, C., 2010, Geologic map of California: California Geological Survey, Geologic Data Map Number 2, scale 1:750,000.

Jiang, D.Z., 2014, Structural geology meets micromechanics: A self-consistent model for the multiscale deformation and fabric development in Earth's ductile lithosphere: Journal of Structural Geology, v. 68, p. 247–272, https://doi.org/10.1016/j.jsg.2014.05.020.

Jiang, D.Z., and Bentley, C., 2012, A micromechanical approach for simulating multiscale fabrics in large-scale high-strain zones: Theory and application: Journal of Geophysical Research, v. 117, B12201, https://doi.org/10.1029/2012JB009327.

Jiang, D.Z., and Williams, P.F., 1999, A fundamental problem with the kinematic interpretation of geological structures: Journal of Structural Geology, v. 21, p. 933–937, https://doi.org/10.1016/S0191-8141(99)00068-1.

Downloaded from http://pubs.geoscienceworld.org/gsa/geosphere/article-pdf/18/6/1752/5737985/ges02478.1.pdf
by San Jose State Univ King Library Periodicals user

Johnson, B.L., 2013, Structure, construction, and emplacement of the Yosemite Valley Intrusive Suite and Yosemite Creek Granodiorite in the central Sierra Nevada batholith [M.S. thesis]: San José, California, San José State University, 95 p., https://doi.org/10.31979/etd.wtyy-e7z3.

Jones, R.R., Holdsworth, R.E., McCaffrey, K.J.W., Clegg, P., and Tavarnelli, E., 2005, Scale dependence, strain compatibility and heterogeneity of three-dimensional deformation during mountain building: A discussion: Journal of Structural Geology, v. 27, p. 1190–1204, https://doi.org/10.1016/j.jsg.2005.04.001.

Karakas, O., Degruyter, W., Bachmann, O., and Dufek, J., 2017, Lifetime and size of shallow magma bodies controlled by crustal-scale magmatism: Nature Geoscience, v. 10, p. 446–450, https://doi.org/10.1038/ngeo2959.

Karlstrom, L., Dufek, J., and Manga, M., 2009, Organization of volcanic plumbing through magmatic lensing by magma chambers and volcanic loads: Journal of Geophysical Research, v. 114, B10204, https://doi.org/10.1029/2009JB006339.

Karlstrom, L., Lee, C.-T.A., and Manga, M., 2014, The role of magmatically driven lithospheric thickening on arc front migration: Geochemistry Geophysics Geosystems, v. 15, p. 2655–2675, https://doi.org/10.1002/2014GC005355.

Kay, S.M., Godoy, E., and Kurtz, A., 2005, Episodic arc migration, crustal thickening, subduction erosion, and magmatism in the south-central Andes: Geological Society of America Bulletin, v. 117, p. 67–88, https://doi.org/10.1130/B25431.1.

Kirsch, M., Paterson, S.R., Wobbe, F., Ardila, A.M.M., Clausen, B.L., and Alasino, P.H., 2016, Temporal histories of Cordilleran continental arcs: Testing models for magmatic episodicity: American Mineralogist, v. 101, p. 2133–2154, https://doi.org/10.2138/am-2016-5718.

Kistler, R.W., 1966, Geologic map of the Mono Craters quadrangle, Mono and Tuolumne Counties, California: U.S. Geological Survey Geologic Quadrangle Map GQ-462, 1 sheet, scale 1:62,500, https://doi.org/10.3133/gq462.

Kistler, R.W., and Peterman, Z.E., 1978, Reconstruction of crustal blocks of California on the basis of initial strontium isotopic compositions of Mesozoic granitic rocks: U.S. Geological Survey Professional Paper 1071, 17 p., https://doi.org/10.3133/pp1071.

Kokkalas, S., and Aydin, A., 2013, Is there a link between faulting and magmatism in the south-central Aegean Sea?: Geological Magazine, v. 150, p. 193–224, https://doi.org/10.1017/S0016756812000453.

Krueger, R.J., and Yoshinobu, A.S., 2018, Structures in the Jackass Lakes pluton–host-rock system, central Sierra Nevada, California, and inferred mid-Cretaceous Farallon–North America plate kinematics: Geological Society of America Bulletin, v. 130, p. 1940–1958, https://doi.org/10.1130/B31992.1.

Lackey, J.S., Valley, J.W., Chen, J.H., and Stockli, D.F., 2008, Dynamic magma systems, crustal recycling, and alteration in the central Sierra Nevada batholith: The oxygen isotope record: Journal of Petrology, v. 49, p. 1397–1426, https://doi.org/10.1093/petrology/egn030.

Lackey, J.S., Cecil, M.R., Windham, C.J., Frazer, R.E., Bindeman, I.N., and Gehrels, G.E., 2012, The Fine Gold Intrusive Suite: The roles of basement terranes and magma source development in the Early Cretaceous Sierra Nevada batholith: Geosphere, v. 8, p. 292–313, https://doi.org/10.1130/GES00745.1.

Leopold, M.B., 2016, Structure, construction, and emplacement of the Late Cretaceous Sonora Pass intrusive suite: Central Sierra Nevada batholith, California [M.S. thesis]: San José, California, San José State University, 95 p., https://doi.org/10.31979/etd.pq8y-gb84.

Lin, S.F., Jiang, D.Z., and William, P.F., 1998, Transpression (or transtension) zones of triclinic symmetry: Natural example and theoretical modelling, *in* Holdsworth, R.E., Strachan, R.A., and Dewey, J.F., eds., Continental Transpressional and Transtensional Tectonics: Geological Society of London Special Publication 135, p. 41–57, https://doi.org/10.1144/GSL.SP.1998.135.01.04.

Lister, G.S., and Williams, P.F., 1983, The partitioning of deformation in flowing rock masses: Tectonophysics, v. 92, p. 1–33, https://doi.org/10.1016/0040-1951(83)90083-5.

Ludwig, K.R., 2012, Isoplot/Ex 3.75: A geochronological toolkit for Microsoft Excel: Berkeley Geochronological Center Special Publication 5, 76 p.

Ma, X.X., Attia, S., Cawood, T.K., Cao, W.R., Xu, Z.Q., and Li, H.B., 2022, Arc tempos of the Gangdese batholith, southern Tibet: Journal of Geodynamics, v. 149, https://doi.org/10.1016/j.jog.2022.101897.

McCaffrey, R., Zwick, P.C., Bock, Y., Prawirodirdjo, L., Genrich, J.F., Stevens, C.W., Puntodewo, S.S.O., and Subarya, C., 2000, Strain partitioning during oblique plate convergence in northern Sumatra: Geodetic and seismologic constraints and numerical modeling: Journal of Geophysical Research, v. 105, p. 28,363–28,376, https://doi.org/10.1029/1999JB900362.

McFarlan, R., 2007, Structure and emplacement of Buena Vista Crest Intrusive Suite, California [M.S. thesis]: San José, California, San José State University, 81 p., https://doi.org/10.31979/etd.3gbf-69mg.

McNulty, B.A., 1995, Shear zone development during magmatic arc construction: The Bench Canyon shear zone, central Sierra Nevada, California: Geological Society of America Bulletin, v. 107, p. 1094–1107, https://doi.org/10.1130/0016-7606(1995)107<1094:SZDDMA>2.3.CO;2.

McNulty, B.A., Tong, W.X., and Tobisch, O.T., 1996, Assembly of a dike-fed magma chamber: The Jackass Lakes pluton, central Sierra Nevada, California: Geological Society of America Bulletin, v. 108, p. 926–940, https://doi.org/10.1130/0016-7606(1996)108<0926:AOADFM>2.3.CO;2.

McNulty, B.A., Tobisch, O.T., Cruden, A.R., and Gilder, S., 2000, Multistage emplacement of the Mount Givens pluton, central Sierra Nevada, California: Geological Society of America Bulletin, v. 112, p. 119–135, https://doi.org/10.1130/0016-7606(2000)112<119:MEOTMG>2.0.CO;2.

Memeti, V., Paterson, S., Matzel, J., Mundil, R., and Okaya, D., 2010a, Magmatic lobes as "snapshots" of magma chamber growth and evolution in large, composite batholiths: An example from the Tuolumne intrusion, Sierra Nevada, California: Geological Society of America Bulletin, v. 122, p. 1912–1931, https://doi.org/10.1130/B30004.1.

Memeti, V., Gehrels, G.E., Paterson, S.R., Thompson, J.M., Mueller, R.M., and Pignotta, G.S., 2010b, Re-evaluating the Mojave–Snow Lake fault hypothesis and origins of central Sierran metasedimentary pendant strata using detrital zircon provenance analyses: Lithosphere, v. 2, p. 341–360, https://doi.org/10.1130/L58.1.

Memeti, V., Paterson, S.R., Economos, R., Erdmann, S., and Miller, R.B., compilers, 2012, Geology of the Benson Lake pendant, western Yosemite National Park, central Sierra Nevada: Geological Society of America Digital Map and Chart Series 13, 1 sheet, scale 1:10,000, 6 p. text, https://doi.org/10.1130/2012.DMCH013.

Memeti, V., Paterson, S.R., and Mundil, R., 2022, Coupled magmatic and host rock processes during the initiation of the Tuolumne Intrusive Complex: A transition from ephemeral sheets to long-lived, active magma mushes: Geological Society of America Bulletin, v. 134, p. 1347–1374, https://doi.org/10.1130/B35871.1.

Miller, R.B., and Paterson, S.R., 1995, Construction of mid-crustal magma chambers during regional contraction, North Cascades, Washington, *in* Brown, M., and Piccoli, P.M., eds., The Origin of Granites and Related Rocks: Third Hutton Symposium Abstracts: U.S. Geological Survey Circular 1129, p. 111–112, https://doi.org/10.3133/cir1129.

Miller, R.B., and Paterson, S.R., 1999, In defense of magmatic diapirs: Journal of Structural Geology, v. 21, p. 1161–1173, https://doi.org/10.1016/S0191-8141(99)00033-4.

Miller, R.B., Paterson, S.R., Lebit, H., Alsleben, H., and Lüneburg, C., 2006, Significance of composite lineations in the mid- to deep crust: A case study from the North Cascades, Washington: Journal of Structural Geology, v. 28, p. 302–322, https://doi.org/10.1016/j.jsg.2005.11.003.

Montanari, D., Giacomo, C., Sani, F., Del Ventisette, C., Bonini, M., and Moratti, G., 2010, Experimental investigation on granite emplacement during shortening: Tectonophysics, v. 484, p. 147–155, https://doi.org/10.1016/j.tecto.2009.09.010.

Mookerjee, M., Canada, A., and Fortescue, F.Q., 2016, Quantifying thinning and extrusions associated with an oblique subduction zone: An example from the Rosy Finch Shear Zone: Tectonophysics, v. 693, p. 290–303, https://doi.org/10.1016/j.tecto.2016.06.012.

Morton, D.M., Miller, F.K., Kistler, R.W., Premo, W.R., Lee, C.-T.A., Langenheim, V.E., Wooden, J.L., Snee, L.W., Clausen, B.L., and Cossette, P., 2014, Framework and petrogenesis of the northern Peninsular Ranges batholith, southern California, *in* Morton, D.M., and Miller, F.K., eds., Peninsular Ranges Batholith, Baja California and Southern California: Geological Society of America Memoir 211, p. 61–143, https://doi.org/10.1130/2014.1211(03).

Mundil, R., Nomade, S., Paterson, S.R., and Renne, P.R., 2004, Geochronological constraints ($^{40}Ar/^{39}Ar$ and U/Pb) on the thermal history of the Tuolumne Intrusive Suite (Sierra Nevada, California): Eos (Transactions, American Geophysical Union), v. 85, no. 47, Fall Meeting Suppl., abstract V53A-0616.

Nadin, E.S., Saleeby, J., and Wong, M., 2016, Thermal evolution of the Sierra Nevada batholith, California, and implications for strain localization: Geosphere, v. 12, p. 377–399, https://doi.org/10.1130/GES01224.1.

Nakamura, K., 1977, Volcanoes as possible indicators of tectonic stress orientation—Principle and proposal: Journal of Volcanology and Geothermal Research, v. 2, p. 1–16, https://doi.org/10.1016/0377-0273(77)90012-9.

Downloaded from http://pubs.geoscienceworld.org/gsa/geosphere/article-pdf/18/6/1752/5737985/ges02478.1.pdf
by San Jose State Univ King Library Periodicals user

Neves, S.P., Vauchez, C., and Archanjo, C.J., 1996, Shear zone–controlled magma emplacement or magma-assisted nucleation of shear zones? Insights from northeast Brazil: Tectonophysics, v. 262, p. 349–364, https://doi.org/10.1016/0040-1951(96)00007-8.

Nomade, S., Mundil, R., Renne, P.R., Onezime, J., and Paterson, S.R., 2003, $^{40}Ar/^{39}Ar$ and U/Pb chronology of the Green Lake pluton (eastern Sierra Nevada, California): Eos (Transactions, American Geophysical Union), v. 86, no. 46, Fall Meeting Suppl., abstract V32C-1039.

Pachell, M.A., and Evans, J.P., 2002, Growth, linkage, and termination processes of a 10-km-long strike-slip fault in jointed granite: The Gemini fault zone, Sierra Nevada, California: Journal of Structural Geology, v. 24, p. 1903–1924, https://doi.org/10.1016/S0191-8141(02)00027-5.

Paterson, S.R., and Ducea, M.N., 2015, Arc magmatic tempos: Gathering the evidence: Elements, v. 11, p. 91–98, https://doi.org/10.2113/gselements.11.2.91.

Paterson, S.R., and Farris, D.W., 2008, Downward host rock transport and the formation of rim monoclines during the emplacement of Cordilleran batholiths: Transactions of the Royal Society of Edinburgh: Earth Sciences, v. 97, p. 397–413, https://doi.org/10.1017/S026359330000153X.

Paterson, S.R., and Fowler, T.K., 1993, Re-examining pluton emplacement processes: Journal of Structural Geology, v. 15, p. 191–206, https://doi.org/10.1016/0191-8141(93)90095-R.

Paterson, S.R., and Miller, R.B., 1998, Magma emplacement during arc-perpendicular shortening: An example from Cascades crystalline core, Washington: Tectonics, v. 17, p. 571–586, https://doi.org/10.1029/98TC01604.

Paterson, S.R., and Schmidt, K.L., 1999, Is there a close spatial relationship between faults and plutons?: Journal of Structural Geology, v. 21, p. 1131–1142, https://doi.org/10.1016/S0191-8141(99)00024-3.

Paterson, S.R., and Tobisch, O.T., 1988, Using pluton ages to date regional deformations: Problems with commonly used criteria: Geology, v. 16, p. 1108–1111, https://doi.org/10.1130/0091-7613(1988)016<1108:UPATDR>2.3.CO;2.

Paterson, S.R., and Tobisch, O.T., 1992, Rates of processes in magmatic arcs: Implications for the timing and nature of pluton emplacement and wall rock deformation: Journal of Structural Geology, v. 14, p. 291–300, https://doi.org/10.1016/0191-8141(92)90087-D.

Paterson, S.R., Tobisch, O.T., and Bhattacharyya, T., 1989, Regional structural and strain analyses of terranes in the Western Metamorphic Belt, Central Sierra Nevada, California: Journal of Structural Geology, v. 11, p. 255–273, https://doi.org/10.1016/0191-8141(89)90066-7.

Paterson, S.R., Fowler, T.K., Jr., Schmidt, K.L., Yoshinobu, A.S., Yuan, E.S., and Miller, R.B., 1998, Interpreting magmatic fabric patterns in plutons: Lithos, v. 44, p. 53–82, https://doi.org/10.1016/S0024-4937(98)00022-X.

Paterson, S.R., Okaya, D., Memeti, V., Economos, R., and Miller, R.B., 2011, Magma addition and flux calculations of incrementally constructed magma chambers in continental margin arcs: Combined field, geochronologic, and thermal modeling studies: Geosphere, v. 7, p. 1439–1468, https://doi.org/10.1130/GES00696.1.

Paterson, S.R., Memeti, V., Anderson, L., Wenrong Cao, Lackey, J.S., Putirka, K.D., Miller, R.B., Miller, J.S., and Mundil, R., 2014, Day 6: Overview of arc processes and tempos, *in* Memeti, V., Paterson, S.R., and Putirka, K.D., eds., Formation of the Sierra Nevada Batholith: Magmatic and Tectonic Processes and Their Tempos: Geological Society of America Field Guide 34, p. 87–116, https://doi.org/10.1130/2014.0034(06).

Paterson, S.R., Memeti, V., Mundil, R., and Žák, J., 2016, Repeated, multiscale, magmatic erosion and recycling in an upper-crustal pluton: Implications for magma chamber dynamics and magma volume estimates: American Mineralogist, v. 101, p. 2176–2198, https://doi.org/10.2138/am-2016-5576.

Paterson, S.R., Ardill, K.E., Vernon, R., and Žák, J., 2019, A review of mesoscopic magmatic structures and their potential for evaluating the hypersolidus evolution of intrusive complexes: Journal of Structural Geology, v. 125, p. 134–147, https://doi.org/10.1016/j.jsg.2018.04.022.

Peck, D.L., 1980, Geologic map of the Merced Peak quadrangle, central Sierra Nevada, California: U.S. Geological Survey Geologic Quadrangle Map GQ-1531, 1 sheet, scale 1:62,5000, https://doi.org/10.3133/gq1531.

Perry-Houts, J., and Karlstrom, L., 2019, Anisotropic viscosity and time-evolving lithospheric instabilities due to aligned igneous intrusions: Geophysical Journal International, v. 216, p. 794–802, https://doi.org/10.1093/gji/ggy466.

Petford, N., Cruden, A.R., McCaffrey, K.J.W., and Vigneresse, J.-L., 2000, Granite magma formation, transport and emplacement in the Earth's crust: Nature, v. 408, p. 669–673, https://doi.org/10.1038/35047000.

Petsche, J.M., 2008, Structure of the Sentinel Granodiorite, Yosemite National Park, California [M.S. thesis]: San José, California, San José State University, 102 p., https://doi.org/10.31979/etd.2nvz-ayns.

Pfiffner, O.A., and Ramsay, J.G., 1982, Constraints on geological strain rates: Arguments from finite strain states of naturally deformed rocks: Journal of Geophysical Research, v. 87, p. 311–321, https://doi.org/10.1029/JB087iB01p00311.

Pignotta, G.S., 2006, Testing models for the incremental growth of magma chambers and coupled displacement of host-rocks during pluton construction with an emphasis on magmatic stoping [Ph.D. thesis]: Los Angeles, University of Southern California, 246 p.

Pignotta, G.S., Paterson, S.R., Coyne, C.C., Anderson, J.L., and Onezime, J., 2010, Processes involved during incremental growth of the Jackass Lakes pluton, central Sierra Nevada batholith: Geosphere, v. 6, p. 130–159, https://doi.org/10.1130/GES00224.1.

Platt, J.P., and Behr, W.M., 2011, Lithospheric shear zones as constant stress experiments: Geology, v. 39, p. 127–130, https://doi.org/10.1130/G31561.1.

Putnam, R., Glazner, A.F., Coleman, D.S., Kylander-Clark, A.R.C., Pavelsky, T., and Abbot, M.I., 2015, Plutonism in three dimensions: Field and geochemical relations on the southeast face of El Capitan, Yosemite National Park, California: Geosphere, v. 11, p. 1133–1157, https://doi.org/10.1130/GES01133.1.

Ratajeski, K., Glazner, A.F., and Miller, B.V., 2001, Geology and geochemistry of mafic to felsic plutonic rocks in the Cretaceous intrusive suite of Yosemite Valley, California: Geological Society of America Bulletin, v. 113, p. 1486–1502, https://doi.org/10.1130/0016-7606(2001)113<1486:GAGOMT>2.0.CO;2.

Ratschbacher, B.C., Keller, C.B., Schoene, B., Paterson, S.R., Anderson, J.L., Okaya, D., Putirka, K., and Lippoldt, R., 2018, A new workflow to assess emplacement duration and melt residence time of compositionally diverse magmas emplaced in a sub-volcanic reservoir: Journal of Petrology, v. 59, p. 1787–1810, https://doi.org/10.1093/petrology/egy079.

Renne, P.R., Tobisch, O.T., and Saleeby, J.B., 1993, Thermochronologic record of pluton emplacement, deformation, and exhumation at Courtright shear zone, central Sierra Nevada, California: Geology, v. 21, p. 331–334, https://doi.org/10.1130/0091-7613(1993)021%3C0331:TROPED%3E2.3.CO;2.

Ruch, J., Vezzoli, L., De Rosa, R., Di Lorenzo, R., and Acocella, V., 2016, Magmatic control along a strike-slip volcanic arc: The central Aeolian arc (Italy): Tectonics, v. 35, p. 407–424, https://doi.org/10.1002/2015TC004060.

Rusmore, M.E., Bogue, S.W., and Woodsworth, G.J., 2013, Paleogeography of the Insular and Intermontane terranes reconsidered: Evidence from the southern Coast Mountains Batholith, British Columbia: Lithosphere, v. 5, p. 521–536, https://doi.org/10.1130/L288.1.

Saleeby, J.B., 1982, Polygenetic ophiolite belt of the California Sierra Nevada: Geochronological and tectonostratigraphic development: Journal of Geophysical Research, v. 87, p. 1803–1824, https://doi.org/10.1029/JB087iB03p01803.

Saleeby, J.B., 1990, Progress in tectonic and petrogenetic studies in an exposed cross-section of young (~100 Ma) continental crust, southern Sierra Nevada, California, *in* Salisbury, M.H., and Fountain, D.M., eds., Exposed Cross-Sections of the Continental Crust: Dordrecht, Kluwer Academic Publishers, p. 137–158, https://doi.org/10.1007/978-94-009-0675-4_6.

Saleeby, J.B., and Dunne, G., 2015, Temporal and tectonic relations of early Mesozoic arc magmatism, southern Sierra Nevada, California, *in* Anderson, T.H., Didenko, A.N., Johnson, C.L., Khanchuk, A.I., and MacDonald, J.H., Jr., eds., Late Jurassic Margin of Laurasia—A Record of Faulting Accommodating Plate Rotation: Geological Society of America Special Paper 513, p. 223–268, https://doi.org/10.1130/2015.2513(05).

Saleeby, J.B., Geary, E.E., Paterson, S.R., and Tobisch, O.T., 1989, Isotopic systematics of Pb/U (zircon) and $^{40}Ar/^{39}Ar$ (biotite-hornblende) from rocks of the central Foothills terrane, Sierra Nevada, California: Geological Society of America Bulletin, v. 101, p. 1481–1492, https://doi.org/10.1130/0016-7606(1989)101<1481:ISOPUZ>2.3.CO;2.

Sauer, K.B., Gordon, S.M., Miller, R.B., Vervoort, J.D., and Fisher, C.M., 2017, Transfer of metasupracrustal rocks to midcrustal depths in the North Cascades continental magmatic arc, Skagit Gneiss Complex, Washington: Tectonics, v. 36, p. 3254–3276, https://doi.org/10.1002/2017TC004728.

Scheland, C., Angulo, A., Memeti, V., Ardill, K.E., and Paterson, S.R., 2018, The Late Cretaceous, migrating Jack Main intrusive complex, central Sierra Nevada, CA: Mapping as a powerful tool for unraveling magmatic histories: Abstract V31F-0188 presented at American Geophysical Union Fall Meeting 2018, Washington, D.C., 10–14 December.

Scheland, C.L., Memeti, V., Angulo, A., Hayward, J.A., and Chambers, M., 2019, Shift from source to system control on pluton compositions recorded in the migrated Jack Main Canyon intrusive suite in the central Sierra Nevada, CA: Geological Society of America Abstracts with Programs, v. 51, no. 5, https://doi.org/10.1130/abs/2019AM-341103.

Downloaded from http://pubs.geoscienceworld.org/gsa/geosphere/article-pdf/18/6/1752/5737985/ges02478.1.pdf
by San Jose State Univ King Library Periodicals user

Schmidt, K.L., Paterson, S.R., Blythe, A.E., and Kopf, C., 2009, Mountain building across a lithospheric boundary during arc construction: The Cretaceous Peninsular Ranges batholith in the Sierra San Pedro Martir of Baja California, Mexico: Tectonophysics, v. 477, p. 292–310, https://doi.org/10.1016/j.tecto.2009.04.020.

Schmidt, W.L., and Platt, J.P., 2018, Subduction, accretion, and exhumation of coherent Franciscan blueschist-facies rocks, northern Coast Ranges, California: Lithosphere, v. 10, p. 301–326, https://doi.org/10.1130/L697.1.

Schweickert, R.A., and Lahren, M.M., 2006, Geologic evolution of Saddlebag Lake pendant, eastern Sierra Nevada, California: Tectonic implications, *in* Girty, G.H., and Cooper, J.D., eds., Using Stratigraphy, Sedimentology, and Geochemistry to Unravel the Geologic History of the Southwestern Cordillera: Pacific Section, SEPM (Society for Sedimentary Geology) Publication 101, p. 27–56.

Schweickert, R.A., Bogen, N.L., Girty, G.H., Hanson, R.E., and Merguerian, C., 1984, Timing and structural expression of the Nevadan orogeny, Sierra Nevada, California: Geological Society of America Bulletin, v. 95, p. 967–969, https://doi.org/10.1130/0016-7606(1984)95<967:TASEOT>2.0.CO;2.

Sharp, W.D., Tobisch, O.T., and Renne, P.R., 2000, Development of Cretaceous transpressional cleavage synchronous with batholith emplacement, central Sierra Nevada, California: Geological Society of America Bulletin, v. 112, p. 1059–1066, https://doi.org/10.1130/0016-7606(2000)112<1059:DOCTCS>2.0.CO;2.

Sheldrake, T., Caricchi, L., and Scutari, M., 2020, Tectonic controls on global variations of large-magnitude explosive eruptions in volcanic arcs: Frontiers of Earth Science, v. 8, 127, https://doi.org/10.3389/feart.2020.00127.

Snow, C.A., and Ernst, W.G., 2008, Detrital zircon constraints on sediment distribution and provenance of the Mariposa Formation, central Sierra Nevada foothills, California, *in* Wright, J.E., and Shervais, J.W., eds., Ophiolites, Arcs, and Batholiths: A Tribute to Cliff Hopson: Geological Society of America Special Paper 438, p. 311–330, https://doi.org/10.1130/2008.2438(11).

Sorensen, S.S., Dunne, G.C., Hanson, R.B., Barton, M.D., Becker, J., Tobisch, O.T., and Fiske, R.S., 1998, From Jurassic shores to Cretaceous plutons: Geochemical evidence for paleoalteration environments of metavolcanic rocks, eastern California: Geological Society of America Bulletin, v. 110, p. 326–343, https://doi.org/10.1130/0016-7606(1998)110<0326:FJSTCP>2.3.CO;2.

Sparks, R.S.J., and Cashman, K.V., 2017, Dynamic magma systems: Implications for forecasting volcanic activity: Elements, v. 13, p. 35–40, https://doi.org/10.2113/gselements.13.1.35.

Spence, D.A., and Turcotte, D.L., 1985, Magma-driven propagation of cracks: Journal of Geophysical Research, v. 90, p. 575–580, https://doi.org/10.1029/JB090iB01p00575.

Stanton-Yonge, A., Griffith, W.A., Cembrano, J., St. Julien, R., and Iturrieta, P., 2016, Tectonic role of margin-parallel and margin-transverse faults during oblique subduction in the Southern Volcanic Zone of the Andes: Insights from Boundary Element Modeling: Tectonics, v. 35, p. 1990–2013, https://doi.org/10.1002/2016TC004226.

Stern, T.W., Bateman, P.C., Morgan, B.A., Newell, M.F., and Peck, D.L., 1981, Isotopic U-Pb ages of zircon from the granitoids of the central Sierra Nevada, California: U.S. Geological Survey Professional Paper 1185, 17 p., https://doi.org/10.3133/pp1185.

Taylor, R.Z., 2004, Structure and petrology of an interpluton screen at May Lake, Yosemite National Park, California [M.S. thesis]: Chapel Hill, University of North Carolina, 60 p.

Taylor, S.R., and McLennan, S.M., 1995, The geochemical evolution of the continental crust: Reviews of Geophysics, v. 33, p. 241–265, https://doi.org/10.1029/95RG00262.

Thacker, J.O., Karlstrom, K.E., Kelley, S.A., Crow, R.S., and Kendall, J.J., 2022, Late Cretaceous time-transgressive onset of Laramide arch exhumation and basin subsidence across northern Arizona–New Mexico, USA, and the role of a dehydrating Farallon flat slab: Geological Society of America Bulletin, https://doi.org/10.1130/B36245.1.

Thompson, J.M., Ball, E.N., Fischer, G.C., Jr., Foley, B.J., Memeti, V., Pignotta, G.S., Paterson, S.R., Anderson, J.L., Matzel, J., and Mundil, R., 2007, Searching for the Mojave–Snow Lake fault: Undergraduate team research at USC: Geological Society of America Abstracts with Programs, v. 39, no. 4, p. 75.

Tibaldi, A., 2005, Volcanism in compressional tectonic settings: Is it possible?: Geophysical Research Letters, v. 32, L06309, https://doi.org/10.1029/2004GL021798.

Tibaldi, A., 2008, Contractional tectonics and magma paths in volcanoes: Journal of Volcanology and Geothermal Research, v. 176, p. 291–301, https://doi.org/10.1016/j.jvolgeores.2008.04.008.

Tibaldi, A., Pasquarè, F., and Tormey, D., 2010, Volcanism in reverse and strike-slip fault settings, *in* Cloetingh, S., and Negendank, J., eds., New Frontiers in Integrated Solid Earth Sciences: Dordrecht, Springer-Verlag, p. 315–348, https://doi.org/10.1007/978-90-481-2737-5_9.

Tikoff, B., and de Saint Blanquat, M., 1997, Transpressional shearing and strike-slip partitioning in the Late Cretaceous Sierra Nevada magmatic arc, California: Tectonics, v. 16, p. 442–459, https://doi.org/10.1029/97TC00720.

Tikoff, B., and Greene, D., 1997, Stretching lineations in transpressional shear zones: An example from the Sierra Nevada Batholith, California: Journal of Structural Geology, v. 19, p. 29–39, https://doi.org/10.1016/S0191-8141(96)00056-9.

Tikoff, B., and Teyssier, C., 1992, Crustal-scale, en echelon "P-shear" tensional bridges: A possible solution to the batholithic room problem: Geology, v. 20, p. 927–930, https://doi.org/10.1130/0091-7613(1992)020<0927:CSEEPS>2.3.CO;2.

Tikoff, B., Davis, M.R., Teyssier, C., de Saint-Blanquat, M., Habert, G., and Morgan, S., 2005, Fabric studies within the Cascade Lake shear zone, Sierra Nevada, California: Tectonophysics, v. 400, p. 209–226, https://doi.org/10.1016/j.tecto.2005.03.003.

Titus, S.J., Clark, R., and Tikoff, B., 2005, Geologic and geophysical investigation of two fine-grained granites, Sierra Nevada Batholith, California: Evidence for structural controls on emplacement and volcanism: Geological Society of America Bulletin, v. 117, p. 1256–1271, https://doi.org/10.1130/B25689.1.

Tobisch, O.T., and Cruden, A.R., 1995, Fracture-controlled magmatic conduits in an obliquely convergent continental magmatic arc: Geology, v. 23, p. 941–944, https://doi.org/10.1130/0091-7613(1995)023<0941:FCMCIA>2.3.CO;2.

Tobisch, O.T., and Fiske, R.S., 1982, Repeated parallel deformation in part of the eastern Sierra Nevada, California and its implications for dating structural events: Journal of Structural Geology, v. 4, p. 177–195, https://doi.org/10.1016/0191-8141(82)90026-8.

Tobisch, O.T., and Paterson, S.R., 1988, Analysis and interpretation of composite foliations in areas of progressive deformation: Journal of Structural Geology, v. 10, p. 745–754, https://doi.org/10.1016/0191-8141(88)90081-8.

Tobisch, O.T., Fiske, R.S., Sacks, S., and Taniguchi, D., 1977, Strain in metamorphosed volcaniclastic rocks and its bearing on the evolution of orogenic belts: Geological Society of America Bulletin, v. 88, p. 23–40, https://doi.org/10.1130/0016-7606(1977)88<23:SIMVRA>2.0.CO;2.

Tobisch, O.T., Saleeby, J.B., and Fiske, R.S., 1986, Structural history of continental volcanic arc rocks, eastern Sierra Nevada, California: A case for extensional tectonics: Tectonics, v. 5, p. 65–94, https://doi.org/10.1029/TC005i001p00065.

Tobisch, O.T., Renne, P.R., and Saleeby, J.B., 1993, Deformation resulting from regional extension during pluton ascent and emplacement, central Sierra Nevada, California: Journal of Structural Geology, v. 15, p. 609–628, https://doi.org/10.1016/0191-8141(93)90151-Y.

Tobisch, O.T., Saleeby, J.B., Renne, R.R., McNulty, B., and Tong, W.S., 1995, Variations in deformation fields during development of a large-volume magmatic arc, central Sierra Nevada, California: Geological Society of America Bulletin, v. 107, p. 148–166, https://doi.org/10.1130/0016-7606(1995)107<0148:VIDFDD>2.3.CO;2.

Tobisch, O.T., Fiske, R.S., Saleeby, J.B., Holt, E., and Sorensen, S.S., 2000, Steep tilting of metavolcanic rocks by multiple mechanisms, central Sierra Nevada, California: Geological Society of America Bulletin, v. 112, p. 1043–1058, https://doi.org/10.1130/0016-7606(2000)112<1043:STOMRB>2.0.CO;2.

Tomek, F., Žák, J., Verner, K., Holub, F.V., Sláma, J., Paterson, S.R., and Memeti, V., 2017, Mineral fabrics in high-level intrusions recording crustal strain and volcano-tectonic interactions: The Shellenbarger pluton, Sierra Nevada, California: Journal of the Geological Society, v. 174, p. 193–208, https://doi.org/10.1144/jgs2015-151.

Tommasi, A., Vauchez, A., Fernandes, L.A.D., and Porcher, C.C., 1994, Magma-assisted strain localization in an orogen-parallel transcurrent zone of southern Brazil: Tectonics, v. 13, p. 421–437, https://doi.org/10.1029/93TC03319.

Tong, W.X., 1994, Nature, physical conditions and time constraints of ductile deformation and pluton emplacement in the Quartz Mountain area, Sierra Nevada, California, and within the Changle-Nanao shear zone, Dongshan area, southeast China [Ph.D. thesis]: Santa Cruz, University of California, 167 p.

Van Dyne, A.L., 2014, Structure and emplacement of Cretaceous plutons, northwest Yosemite National Park, California [M.S. thesis]: San José, California, San José State University, 74 p., https://doi.org/10.31979/etd.akfj-5ha8.

Vernon, R.H., 2000, Review of microstructural evidence of magmatic and solid-state flow: Visual Geosciences, v. 5, p. 1–23, https://doi.org/10.1007/s10069-000-0002-3.

Vigneresse, J.L., and Clemens, J.D., 2000, Granitic magma ascent and emplacement: Neither diapirism nor neutral buoyancy, *in* Vendeville, B.C., Mart, Y., and Vigneresse, J.-L., eds., Salt, Shale and Igneous Diapirs in and around Europe: Geological Society of London Special Publication 174, p. 1–19, https://doi.org/10.1144/GSL.SP.1999.174.01.01.

Downloaded from http://pubs.geoscienceworld.org/gsa/geosphere/article-pdf/18/6/1752/5737985/ges02478.1.pdf
by San Jose State Univ King Library Periodicals user

Ward, K.M., Zandt, G., Beck, S.L., Christensen, D.H., and McFarlin, H., 2014, Seismic imaging of the magmatic underpinnings beneath the Altiplano-Puna volcanic complex from the joint inversion of surface wave dispersion and receiver functions: Earth and Planetary Science Letters, v. 404, p. 43–53, https://doi.org/10.1016/j.epsl.2014.07.022.

Yang, J.M., Cao, W.R., Gordon, S.M., and Chu, X., 2020, Does underthrusting crust feed magmatic flare-ups in continental arcs?: Geochemistry Geophysics Geosystems, v. 21, https://doi.org/10.1029/2020GC009152.

Yonkee, W.A., and Weil, A.B., 2015, Tectonic evolution of the Sevier and Laramide belts within the North American Cordillera orogenic system: Earth-Science Reviews, v. 150, p. 531–593, https://doi.org/10.1016/j.earscirev.2015.08.001.

Yoshinobu, A.S., Okaya, D.A., and Paterson, S.R., 1998, Modeling the thermal evolution of fault-controlled magma emplacement models: Implications for the solidification of granitoid plutons: Journal of Structural Geology, v. 20, no. 9/10, p. 1205–1218.

Yoshinobu, A.S., Wolak, J.M., Paterson, S.R., Pignotta, G.S., and Anderson, H.S., 2009, Determining relative magma and host rock xenolith rheology during magmatic fabric formation in plutons: Examples from the middle and upper crust: Geosphere, v. 5, p. 270–285, https://doi.org/10.1130/GES00191.1.

Žák, J., Paterson, S.R., and Memeti, V., 2007, Four magmatic fabrics in the Tuolumne batholith, central Sierra Nevada, California (USA): Implications for interpreting fabric patterns in plutons and evolution of magma chambers in the upper crust: Geological Society of America Bulletin, v. 119, p. 184–201, https://doi.org/10.1130/B25773.1.

Downloaded from http://pubs.geoscienceworld.org/gsa/geosphere/article-pdf/18/6/1752/5737985/ges02478.1.pdf
by San Jose State Univ King Library Periodicals user